

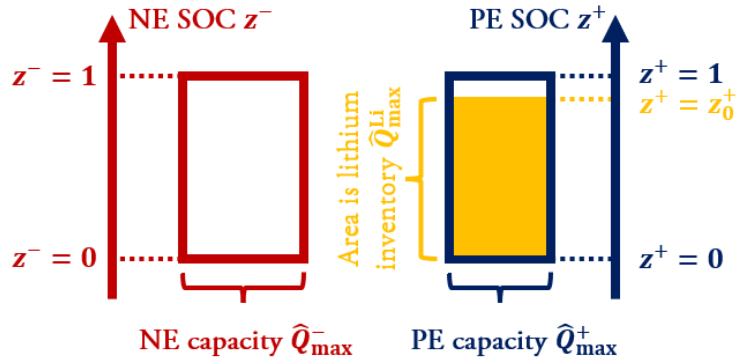
Graphical Abstract

Identifiability Study of Lithium-Ion Battery Capacity Fade Using Degradation Mode Sensitivity for a Minimally and Intuitively Parametrized Electrode-Specific Cell Open-Circuit Voltage Model

Jing Lin, Edwin Khoo

$$U_{OCV} = U_{OCV}^+(z^+) - U_{OCV}^-(z^-); \quad z^+ = z_0^+ - r_{N/P} z^-$$

$$N/P \text{ ratio: } r_{N/P} = \frac{\hat{Q}_{max}^-}{\hat{Q}_{max}^+}; \quad Li/P \text{ ratio: } z_0^+ = \frac{\hat{Q}_{max}^{Li}}{\hat{Q}_{max}^+}$$



## Highlights

### **Identifiability Study of Lithium-Ion Battery Capacity Fade Using Degradation Mode Sensitivity for a Minimally and Intuitively Parametrized Electrode-Specific Cell Open-Circuit Voltage Model**

Jing Lin, Edwin Khoo

- An electrode-specific OCV model parametrized by N/P and Li/P ratio.
- Degradation modes and electrode SOC based on material-specific usable stoichiometry range.
- Electrode differential voltage fractions indicating the limiting electrode.
- Four regimes of degradation identifiability characterized by Li/N and Li/P ratio.
- Informative SOC windows for degradation mode estimation by Fisher information.

# Identifiability Study of Lithium-Ion Battery Capacity Fade Using Degradation Mode Sensitivity for a Minimally and Intuitively Parametrized Electrode-Specific Cell Open-Circuit Voltage Model

Jing Lin<sup>a</sup>, Edwin Khoo<sup>a,\*</sup>

<sup>a</sup>*Institute for Infocomm Research (I2R), Agency for Science, Technology and Research (A\*STAR), 1 Fusionopolis Way, #21-01 Conneris South, Singapore 138632, Republic of Singapore*

---

## Abstract

When two electrode open-circuit potentials form a full-cell OCV (open-circuit voltage) model, cell-level SOH (state of health) parameters related to LLI (loss of lithium inventory) and LAM (loss of active materials) naturally appear. Such models have been used to interpret experimental OCV measurements and infer these SOH parameters associated with capacity fade. In this work, we first re-parametrize a popular OCV model formulation by the N/P (negative-to-positive) ratio and Li/P (lithium-to-positive) ratio, which have more symmetric and intuitive physical meaning, and are also pristine-condition-agnostic and cutoff-voltage-independent. We then study the modal identifiability of capacity fade by mathematically deriving the gradients of electrode slippage and cell OCV with respect to these SOH parameters, where the electrode differential voltage fractions, which characterize each electrode's relative contribution to the OCV slope, play a key role in passing the influence of a fixed cutoff voltage to the parameter sensitivity. The sensitivity gradients of the total capacity also reveal four characteristic regimes regarding how much lithium inventory and active materials are limiting the apparent capacity. We show the usefulness of these sensitivity gradients with an application regarding degradation mode identifiability from OCV measurements at different SOC (state of charge) windows.

*Keywords:* Lithium-ion battery, loss of active materials, loss of lithium inventory, open-circuit voltage, parametric identifiability, sensitivity gradient

---

## 1. Introduction: Characterizing Degradation by SOH parameters

Lithium-ion batteries degrade over time upon operation and storage due to many complex and coupled physicochemical mechanisms and processes [1, 2]. Degradation causes a battery cell to lose capacity and rate capability, where the former represents charge throughput between the cell's fully charged and discharged state, while the latter indicates the maximum charge/discharge C-rate the cell can withhold within a short period. These two aspects of aging are usually called capacity and power fade, respectively [3].

One technical subtlety here is that the fully charged and discharged state is defined by the cell OCV (open-circuit voltage) reaching a pre-specified upper and lower cutoff voltage  $U_{\max}$  and  $U_{\min}$ , respectively, and the charge throughput between these two states is named the total capacity  $\hat{Q}_{\max}$  and is what capacity fade specifically concerns [4]. However, under finite-current operation,

---

\*Corresponding author.

*Email addresses:* [lin\\_jing@ihpc.a-star.edu.sg](mailto:lin_jing@ihpc.a-star.edu.sg) (Jing Lin), [edwin\\_khoo@ihpc.a-star.edu.sg](mailto:edwin_khoo@ihpc.a-star.edu.sg) (Edwin Khoo)

the observed terminal voltage shall reach a cutoff voltage before the underlying OCV does due to polarization in non-equilibrium, so the commonly reported charge/discharge capacity during cycling can be significantly smaller than the total capacity, unless both charging and discharging have a trailing CV (constant-voltage) phase with a small enough cutoff current. The key is that the cell must have reached quasi-equilibrium at  $U_{\max}$  and  $U_{\min}$  before and after the Coulomb counting, respectively. The total capacity depends only on the thermodynamic properties of the cell, while the charge/discharge capacity also depends on the kinetic characteristics and operation protocols. Therefore, the latter’s reduction upon aging is due to both capacity and power fade. It is not uncommon to see a charge/discharge capacity being confused with the total capacity in literature, but the distinction is important for the various modes of capacity fade.

A battery cell’s voltage response to an input current profile can be captured and predicted by a cell model, be it physics-based and derived from first principles, or semi-empirical and approximated by an equivalent circuit [4]. Therefore, within such a model, a cell’s capacity and rate capability are completely encoded by certain model parameters, which we will refer to as SOH (state of health) parameters, and the granularity of this parametrization depends on the model’s complexity. Such SOH parameters interface between the underlying physicochemical degradation mechanisms and the apparent cell performance metrics, so the performance decay caused by the change of a particular parameter is also called a degradation mode [3]. If such SOH parameters can be identified from observed cell behaviors, we can track how they evolve across a cell’s lifetime under different operating conditions, which might provide valuable clues about dominant aging mechanisms, inspire the formulation of more accurate degradation models, enable more effective aging-aware battery management and control, and even guide battery design to attenuate degradation.

Although we treat SOH here as a loose term that denotes a cell’s capacity and rate capability, whose precise meaning depends on the context of a particular cell model, SOH historically often refers to the total capacity  $\hat{Q}_{\max}$  and equivalent internal resistance  $R_0$  of a cell [5], which form possibly the coarsest-grained description of capacity and power fade, and correspond to a simple ECM (equivalent circuit model) with only a monolithic OCV source  $U_{\text{OCV}}(z)$  assumed to be unchanged upon aging [6] and a series resistor of  $R_0$ . Here  $z$  denotes the cell SOC (state of charge), whose precise meaning will be clarified in section 2.2, and we will use the  $\hat{Q}$  notation with a hat for any capacity whose definition relies on specifying an upper and lower cutoff voltage or potential for a full cell or an electrode, respectively. There has been an enormous amount of research dedicated to estimating  $\hat{Q}_{\max}$  and  $R_0$  from voltage and current measurements [5, 7], but such parametrization is too coarse-grained to shed light on possible underlying degradation mechanisms. In this work, we will restrict ourselves to capacity fade only and focus on a natural refinement of the monolithic OCV relation by constructing the cell OCV as the difference between the PE (positive electrode/cathode) and NE (negative electrode/anode) OCP (open-circuit potential):

$$U_{\text{OCV}}(z^-, z^+) = U_{\text{OCP}}^+(z^+) - U_{\text{OCP}}^-(z^-), \quad (1)$$

where  $z^\pm$  are the PE and NE SOC to be defined in section 2.1, and three SOH parameters lithium inventory  $\hat{Q}_{\max}^{\text{Li}}$ , PE active materials  $\hat{Q}_{\max}^+$ , and NE active materials  $\hat{Q}_{\max}^-$ , all measured in charges, will naturally surface in place of a single total capacity  $\hat{Q}_{\max}$  as the SOH parameters, which correspond to the three well-known capacity fade modes: LLI (loss of lithium inventory), LAMP, and LAMn (loss of active materials in PE/NE), respectively [8].

The development history of the above electrode-specific OCV model, though with different parametrization, has recently been reviewed by Olson et al. [9] under the context of DV (differential voltage) and IC (incremental capacity) analysis. Indeed, this model was used to estimate the three

modes of capacity fade first by DV [10] and IC [8, 9] analysis, based on the parametrization

$$U_{\text{OCV}}(z^-) = U_{\text{OCP}}^+(1 - (b_{\text{OFS}} + a_{\text{LR}}z^-)) - U_{\text{OCP}}^-(z^-), \quad (2)$$

where the loading ratio  $a_{\text{LR}}$  is the familiar NE-to-PE capacity ratio, while  $b_{\text{OFS}}$  is interpreted as the loss of lithium inventory scaled by PE capacity. However, DV and IC analysis is not yet a fully automatic technique, and they require users to judge how the peaks and troughs of the full-cell DV and IC curves are associated with electrode OCP features [9]. Later, researchers attempted to estimate the three modes of LLI, LAMn, and LAMp directly by fitting the model OCV curve to experimental measurements using classical NLS (nonlinear least squares) [3, 11]. In particular, Birkl et al. [3] experimentally validate this approach by assembling coin cells with a controlled amount of lithium inventory and active materials, which serve as the ground truth against optimization results from NLS. However, they parametrize their electrode-specific OCV

$$U_{\text{OCV}}(z) = U_{\text{OCP}}^+(z_{\text{max}}^+ - z(z_{\text{max}}^+ - z_{\text{min}}^+)) - U_{\text{OCP}}^-(z_{\text{min}}^- + z(z_{\text{max}}^- - z_{\text{min}}^-)) \quad (3)$$

by the extreme electrode SOC  $z_{\text{max}}^\pm$  and  $z_{\text{min}}^\pm$ , which are constrained by the upper and lower cutoff voltage and have rather complicated dependence on the three modes. Mohtat et al. [11] instead use the OCV in terms of the discharge throughput  $Q_d$  counted from the fully charged state:

$$U_{\text{OCV}}(Q_d) = U_{\text{OCP}}^+(z_{\text{min}}^+ + Q_d/\hat{Q}_{\text{max}}^+) - U_{\text{OCP}}^-(z_{\text{max}}^- - Q_d/\hat{Q}_{\text{max}}^-), \quad (4)$$

which is parametrized by  $z_{\text{min}}^+$ ,  $z_{\text{max}}^-$ , and  $\hat{Q}_{\text{max}}^\pm$ , subject to the constraint  $U_{\text{OCP}}^+(z_{\text{min}}^+) - U_{\text{OCP}}^-(z_{\text{max}}^-) = U_{\text{max}}$ . They also derive the gradient of  $U_{\text{OCV}}(Q_d)$  with respect to the four parameters and use Fisher information to quantify the parametric identifiability. This OCV model has been incorporated in PyBaMM [12], an open battery modeling package implemented in Python, and much subsequent work on model-based degradation mode estimation has used different variants of this four-parameter formulation [13, 14].

In this work, we argue that the parametrization (3) or (4) based on electrode SOC at a certain cutoff voltage involves non-independent parameters, of which the redundancy complicates their estimation. Moreover, the cutoff voltage is an operational parameter that is not intrinsic to the aging state of a cell, so a parametrization that depends on it blurs the intrinsic degradation trend and makes the SOH parameters less intuitive to interpret. We also argue not to parametrize the OCV by the LLI, LAMn and LAMp percentage, as these quantities rely on specifying the pristine-cell SOH parameters, which are irrelevant to the current SOH and could be arbitrary. Instead, these percentage losses should be defined in terms of the SOH parameters and their values for a pristine cell [9], and only calculated as derived quantities when needed and available.

Here, we slightly re-parametrize (2) by the N/P (negative-to-positive) ratio  $r_{\text{N/P}} = \hat{Q}_{\text{max}}^-/\hat{Q}_{\text{max}}^+$  and the Li/P (lithium-to-positive) ratio  $z_0^+ = \hat{Q}_{\text{max}}^{\text{Li}}/\hat{Q}_{\text{max}}^+$ , which have more symmetric and readily interpretable physical meaning, leading to further insights not yet revealed in previous work using (2). This parametrization also implies that the discharge-count-based OCV  $U_{\text{OCV}}(Q_d)$  depends only on three SOH parameters: lithium inventory  $\hat{Q}_{\text{max}}^{\text{Li}}$ , NE active materials  $\hat{Q}_{\text{max}}^-$ , and PE active materials  $\hat{Q}_{\text{max}}^+$ , all measured in equivalent charges. These parameters are independent, do not depend on any full-cell cutoff voltage or pristine-cell SOH, and their changes directly and intuitively capture the three modes of LLI, LAMn, and LAMp. Moreover, after the upper and lower cutoff voltage of a cell are specified to define the cell SOC  $z$ , the SOC-based OCV  $U_{\text{OCV}}(z)$  only depends on two independent dimensionless parameters of Li/P and N/P ratio. Along the way, we will also clarify several common misconceptions regarding the use of an electrode-specific OCV model.

We will further analytically derive the gradients of  $U_{\text{OCV}}(z)$ ,  $U_{\text{OCV}}(Q_d)$ , and total capacity  $\hat{Q}_{\text{max}}$  with respect to the SOH parameters, and demonstrate the further insights provided by this sensitivity analysis beyond what has been shown in [11, 15]. In particular, we will introduce the electrode DV (differential voltage) fraction, which is instrumental in channeling the effects of a fixed upper and lower cutoff voltage into the sensitivity gradients. The analytic results will also be visualized, verified, and corroborated by simulations. Note that as shown in section 2.4, this DV fraction is closely related to  $dU_{\text{OCP}}^{\pm}/dz^{\pm}$  and  $dU_{\text{OCV}}/dz$ , which are also the central objects in DV analysis [16, 9], but to be clear, this work is not related to DV analysis.

Finally, we will also present a direct application of our analytic results, where the sensitivity gradients are fed to the Fisher information matrix to quantify the identifiability of the Li/P and N/P ratio from measurements of the SOC-based  $U_{\text{OCV}}(z)$  and to quantify the identifiability of the lithium inventory and active material amounts from partial charge-based OCV measurements.

Note that there have been much work on adapting an OCV model to degradation mode estimation under more realistic scenarios such as with finite current or composite electrodes [17, 18], as well as extracting certain OCV features as better health indicators [19], but these are all built upon a baseline electrode-specific OCV model. This work is not about a more advanced estimation algorithm, but presents a more compact and intuitive parametrization that can be substituted into any such algorithm. Moreover, this parametrization also leads to further insights into how the cell OCV and capacity depend on these SOH parameters and degradation modes, which can guide us even in more complicated situations.

## 2. Methodology and Analysis

Before diving into the degradation mode parametrization and identifiability, we want to clarify a few concepts that could be ambiguous in literature.

### 2.1. Electrode OCP: Stoichiometry, Electrode SOC and Active Material Amount

For a lithium intercalation electrode, the stoichiometry  $x$  is literally the stoichiometric coefficient of lithium in the active material chemical formula that indicates the lithiation state, usually with  $0 \leq x \leq 1$  such as in graphite  $\text{Li}_x\text{C}_6$  and LFP (lithium iron phosphate)  $\text{Li}_x\text{FePO}_4$ , where  $x = 0$  and  $x = 1$  corresponds to the theoretical fully delithiated and lithiated state, respectively. The chemical formula also yields the theoretical electrode specific capacity, such as  $q_{\text{max}}^- = 372$  mAh/g for  $\text{Li}_x\text{C}_6$  and  $q_{\text{max}}^+ = 170$  mAh/g for  $\text{Li}_x\text{FePO}_4$ , where  $q_{\text{max}}$  denotes gravimetric specific capacity of dimension charge per unit mass, while  $Q_{\text{max}}$  for absolute capacity of charge dimension. In the following, we will use the superscript  $+$  and  $-$  to indicate quantities associated with PE and NE active materials, respectively.

An ideal open-circuit potential relation  $U_{\text{OCP}}^{\pm}(x^{\pm})$  is with respect to the stoichiometry  $x^{\pm}$ , where the potential is measured against the standard lithium metal electrode. However, due to material instability and electrochemical side reactions in practice, we cannot fully lithiate or delithiate an electrode. Besides, we also lack means to directly measure the electrode stoichiometry  $x^{\pm}$ , unless we start from a pristine electrode with a precisely known amount of active materials, which implies  $x^- = 0$  for NE materials like graphite or  $x^+ = 1$  for PE materials like LFP initially, and we can use Coulomb counting and the active material mass to deduce subsequent lithiation states.

In most cases, we can only lithiate/delithiate an electrode (half cell) across a usable potential window and obtain  $U_{\text{OCP}}^{\pm}(Q^{\pm})$  from voltage measurements and Coulomb counting. We only know that the charge throughput  $Q^{\pm}$  is linearly related to  $x^{\pm}$ , but we have no access to the slope and intercept. Hence, the best we can do is to define an electrode SOC  $z^{\pm} \in [0, 1]$  such that  $z^{\pm} = 0$

corresponds to some unknown  $x_{\min}^{\pm}$  at the top of the usable potential window, while  $z^{\pm} = 1$  corresponds to some unknown  $x_{\max}^{\pm}$  at the bottom. This way, we can map  $Q^{\pm}$  linearly to  $z^{\pm}$  and obtain the most commonly seen OCP relations  $U_{\text{OCP}}^{\pm}(z^{\pm})$ . Here we define  $Q^{\pm}$  and the electrode SOC  $z^{\pm}$  to count positively in the lithiation direction corresponding to a cathodic current. We deviate from the convention in general electrochemistry of treating anodic current as positive to correlate  $Q^{\pm}$  and  $z^{\pm}$  with the amount of lithium intercalated, which we find more intuitive in the case of an intercalation electrode. There is also work that defines electrode SOC to be negatively correlated with stoichiometry and positively correlated with electrode potential [8].

The Coulomb counting also tells us the charge throughput associated with the whole interval of  $0 \leq z^{\pm} \leq 1$ , which is the usable electrode capacity  $\hat{Q}_{\max}^{\pm}$ . Note that

$$\hat{Q}_{\max}^{\pm} = (x_{\max}^{\pm} - x_{\min}^{\pm})Q_{\max}^{\pm} \quad (5)$$

can be much smaller than the theoretical electrode capacity  $Q_{\max}^{\pm}$  associated with  $0 \leq x^{\pm} \leq 1$ , and without knowing the active material mass, we cannot obtain  $Q_{\max}^{\pm}$ . Moreover, since  $z^{\pm}$  also relates linearly to  $x^{\pm}$ , we must have

$$z^{\pm} = \frac{x^{\pm} - x_{\min}^{\pm}}{x_{\max}^{\pm} - x_{\min}^{\pm}}, \quad (6)$$

although we do not know these stoichiometry limits in general. See figure 1 in the Supporting Information for an illustration of the connection and distinction between stoichiometry and electrode SOC.

Note also that mathematically, the choice of this upper and lower cutoff potential for defining  $z^{\pm} = 0$  and  $z^{\pm} = 1$ , respectively, is arbitrary, as long as  $\hat{Q}_{\max}^{\pm}$  is scaled accordingly and remains consistent with it, and it will not affect the validity of the following full-cell analysis. That is also why not knowing the stoichiometry  $x^{\pm}$  is not an issue except when we want to correlate electrode behaviors with certain lattice arrangement at a particular  $x^{\pm}$ . However, we want  $U_{\text{OCP}}^{\pm}(z^{\pm})$  to be defined for all of  $0 \leq z^{\pm} \leq 1$ ,  $z^{\pm}$  to intuitively indicate whether the electrode is in a safe operation range, and  $\hat{Q}_{\max}^{\pm}$  to faithfully reflect the usable electrode capacity, so we do need to specify this potential window explicitly and reasonably. We advocate that researchers do not use the term stoichiometry and electrode SOC interchangeably and should report the upper and lower cutoff potential when presenting an OCP curve  $U_{\text{OCP}}^{\pm}(z^{\pm})$ .

Since in general, the active material mass is not available, we propose to use the usable electrode capacity  $\hat{Q}_{\max}^{\pm}$  associated with a certain  $U_{\text{OCP}}^{\pm}(z^{\pm})$  to characterize the amount of active materials in each electrode and the corresponding degradation modes of LAMp and LAMn.

## 2.2. Cell OCV: Cutoff Voltage, Cell SOC, and Degradation Mode Parametrization

When the PE and NE are assembled into a full cell, their respective electrode SOC are no longer independent, but are constrained by charge conservation. Assuming no LLI or LAM, we have

$$z^{+}(z^{-}) = z_0^{+} - r_{\text{N/P}}z^{-}, \quad r_{\text{N/P}} = \frac{\hat{Q}_{\max}^{-}}{\hat{Q}_{\max}^{+}}, \quad z_0^{+} = \frac{\hat{Q}_{\max}^{\text{Li}}}{\hat{Q}_{\max}^{+}}, \quad (7)$$

where the negative slope  $r_{\text{N/P}}$  is the commonly seen N/P (negative-to-positive) ratio, while the intercept  $z_0^{+} = z^{+}(z^{-} = 0)$  is analogously called the Li/P ratio (lithium-to-positive) ratio, since

$$z_0^{+} = \frac{z^{+}\hat{Q}_{\max}^{+} + z^{-}\hat{Q}_{\max}^{-}}{\hat{Q}_{\max}^{+}} = \frac{\hat{Q}_{\max}^{\text{Li}}}{\hat{Q}_{\max}^{+}}. \quad (8)$$

The lithium inventory  $\hat{Q}_{\max}^{\text{Li}}$  essentially accounts for the lithium in both electrodes beyond  $z^{\pm} = 0$ , which is consistent with how  $\hat{Q}_{\max}^{\pm}$  are defined. Note also that the slope  $r_{\text{N/P}}$  and intercept  $z_0^+$  fully characterize the relative slippage between  $z^{\pm}$ . Figure 1a illustrates the physical meaning of these parameters. Figure 2 in the Supporting Information provides further schematics illustrating the fully discharged and charged state.

Substituting eq. (7) into eq. (1), we obtain the  $z^-$ -based full-cell OCV as

$$U_{\text{OCV}}(z^-) = U_{\text{OCP}}^+(z_0^+ - r_{\text{N/P}}z^-) - U_{\text{OCP}}^-(z^-). \quad (9)$$

We can also equivalently relate  $U_{\text{OCV}}$  to  $z^+$ , but  $z^+$  is negatively correlated with the conventionally defined cell SOC  $z$ , and it flips the well adopted N/P ratio to the denominator of the slope.

Assuming that the PE and NE OCP remain unchanged upon degradation, the above electrode-specific OCV model is parametrized by only two independent and dimensionless parameters N/P ratio  $r_{\text{N/P}}$  and Li/P ratio  $z_0^+$ , which have a simple and intuitive physical meaning that links to degradation modes. Also, we have not yet introduced any cutoff voltage for the full cell, so  $U_{\text{OCV}}(z^-)$  together with its two parameters are independent of that choice, and we next show that this parametrization persists even at the presence of a cutoff voltage.

One caveat of assuming an invariant electrode OCP is that crystal structural transformation undergone by certain active materials upon aging that might affect the electrode potential is not captured. Besides, the form of electrode OCP used in this work has also not accounted for competing reactions that might become thermodynamically favorable beyond certain electrode potential threshold, of which the most prominent example is lithium plating when  $U_{\text{OCP}}^-(z^-)$  reaches 0 V. However, these layers of complexities can be laid upon the framework of analysis proposed in this work when needed. For example, see [20] and references therein for a review of techniques to incorporate some of such complexities into OCV modeling.

Note that our N/P ratio  $r_{\text{N/P}}$  and Li/P ratio  $z_0^+$  essentially correspond to the ‘‘loading ratio’’ and ‘‘offset’’ in (2) used in [8, 9] by  $r_{\text{N/P}} = a_{\text{LR}}$  and  $z_0^+ = 1 - b_{\text{OFS}}$ , respectively. However, previous researchers using (2) typically express  $a_{\text{LR}}$  and offset  $b_{\text{OFS}}$  in terms of at least three degradation modes (e.g. equation (5) and (8') in [8]) and sweep each degradation mode using the latter less compact parametrization. Here we will perform parametric study directly on the minimal and intuitive parametrization based on the N/P and Li/P ratio.

In principle, we can charge and discharge a cell until one of the electrodes reaches  $z^{\pm} = 0$  or  $z^{\pm} = 1$ , but in practice, we do not typically get to monitor the two electrode potentials in a full cell as with a three-electrode setup, so instead, we specify a terminal voltage range  $[U_{\min}, U_{\max}]$  for a full cell to operate within, such that either electrode is still prevented from over- or under-lithiation. Hence, define  $z_{\min}^-$  and  $z_{\max}^-$ , which correspond to  $z_{\max}^+$  and  $z_{\min}^+$  by eq. (7), respectively, such that

$$U_{\text{OCV}}(z_{\min}^-) = U_{\min}, \quad U_{\text{OCV}}(z_{\max}^-) = U_{\max}, \quad (10)$$

and call  $U_{\text{OCV}} = U_{\min}$  and  $U_{\text{OCV}} = U_{\max}$  the fully discharged and charged state, respectively. For convenience, we can additionally define the full-cell SOC  $z$  as

$$z = \frac{z^- - z_{\min}^-}{z_{\max}^- - z_{\min}^-} = \frac{z^+ - z_{\max}^+}{z_{\min}^+ - z_{\max}^+}, \quad (11)$$

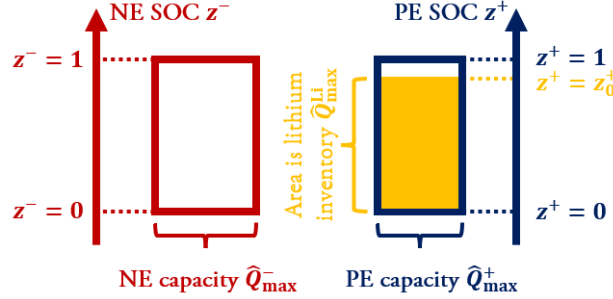
which now exactly traverses [0%, 100%] when  $U_{\text{OCV}}$  ranges between  $U_{\min}$  and  $U_{\max}$ . Substituting  $z^-(z)$  from (11) into the  $z^-$ -based OCV (9), we finally obtain the familiar  $z$ -based OCV:

$$U_{\text{OCV}}(z) = U_{\text{OCP}}^+(z^+(z^-)) - U_{\text{OCP}}^-(z^-(z)). \quad (12)$$

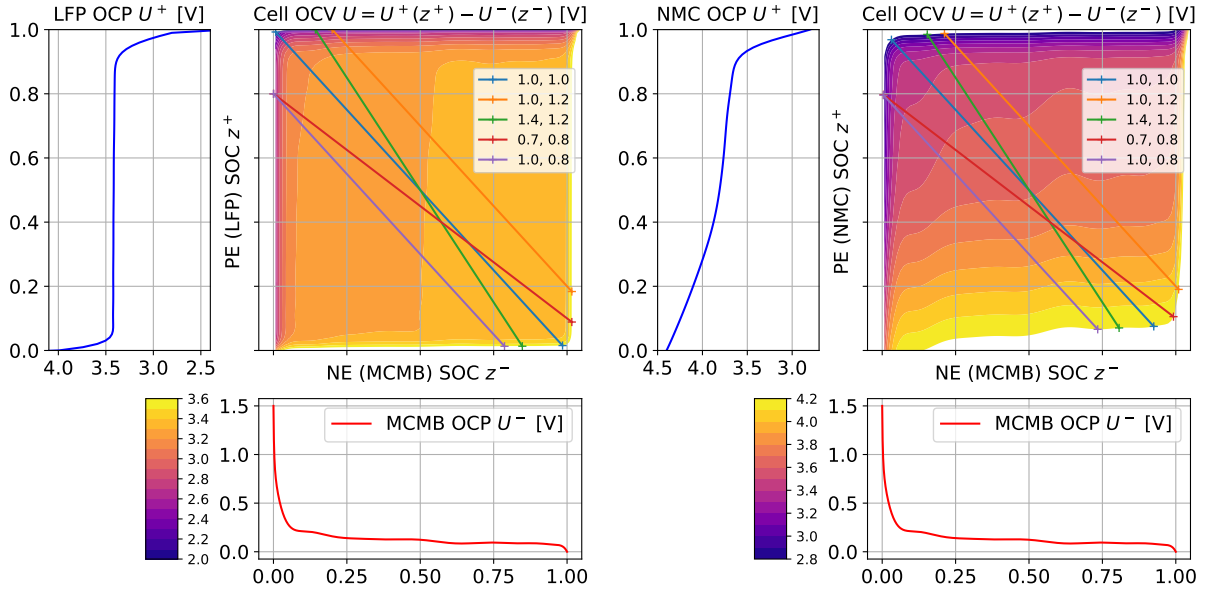


$$U_{\text{OCV}} = U_{\text{OCP}}^+(z^+) - U_{\text{OCP}}^-(z^-); \quad z^+ = z_0^+ - r_{\text{N/P}} z^-$$

$$\text{N/P ratio: } r_{\text{N/P}} = \frac{\hat{Q}_{\text{max}}^-}{\hat{Q}_{\text{max}}^+}; \quad \text{Li/P ratio: } z_0^+ = \frac{\hat{Q}_{\text{max}}^{\text{Li}}}{\hat{Q}_{\text{max}}^+}$$

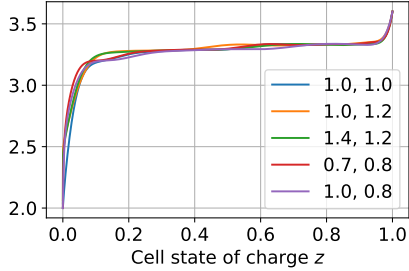


(a) Schematic of an electrode-specific OCV model

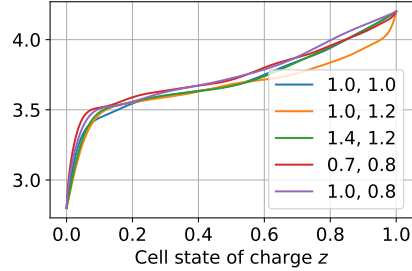


(b) LFP/MCMB:  $U_{\text{OCV}}(z^-, z^+)$   
OCV [V] (N/P, Li/P)

(c) NMC/MCMB:  $U_{\text{OCV}}(z^-, z^+)$   
OCV [V] (N/P, Li/P)



(d) LFP/MCMB:  $U_{\text{OCV}}(z; r_{\text{N/P}}, z_0^+)$



(e) NMC/MCMB:  $U_{\text{OCV}}(z; r_{\text{N/P}}, z_0^+)$

Figure 1: **(a)** A schematic of the OCV model. **(b-e)** The assembly of electrode OCPs into a full-cell OCV, as well as how this assembly is affected by the N/P ratio  $r_{\text{N/P}}$  and Li/P ratio  $z_0^+$ . **(b)** OCV square plots (advocated by Olson et al. [9]) of the LFP-graphite cell chemistry overlaid with five lines of  $z^+(z^-)$  corresponding to cells with different  $(r_{\text{N/P}}, z_0^+)$  pairs as indicated by the legends. Note that the color bar is associated with the contours. **(d)** Various  $z$ -based OCV curves with different  $(r_{\text{N/P}}, z_0^+)$  pairs, which can be considered read off from the contour values on the respective lines in (b). **(c, e)** Counterparts of (b) and (d) for the NMC-graphite chemistry.

Note that eq. (10) essentially comes from the inverse function  $z^-(U_{\text{OCV}})$  defined by (9) evaluated at  $U_{\text{min}}$  and  $U_{\text{max}}$  and is hence also parametrized by  $r_{\text{N/P}}$  and  $z_0^+$ . Therefore, the  $z^-(z)$  from (11) and hence  $U_{\text{OCV}}(z)$  are parametrized by  $r_{\text{N/P}}$ ,  $z_0^+$ ,  $U_{\text{min}}$ , and  $U_{\text{max}}$ , where given  $U_{\text{min}}$  and  $U_{\text{max}}$  fixed,  $U_{\text{OCV}}(z)$  is thus again parametrized by the independent and dimensionless  $r_{\text{N/P}}$  and  $z_0^+$  only. This is the main difference from the parametrization of (3) based on four electrode SOC limits and two cutoff-voltage constraints [3].

			MCMB	LFP	NMC111
$x^\pm = x_{\text{min}}^\pm$	$z^\pm = 0$	$U_{\text{max}}^\pm$ [V]	1.5	4.0	4.4
$x^\pm = x_{\text{max}}^\pm$	$z^\pm = 1$	$U_{\text{min}}^\pm$ [V]	0.0	2.5	2.8

Table 1: Upper and lower cutoff potential specified for each electrode chemistry used in this work.

				LFP/MCMB	NMC/MCMB
$z^- = z_{\text{max}}^-$	$z^+ = z_{\text{min}}^+$	$z = 1$	$U_{\text{max}}$ [V]	3.6	4.2
$z^- = z_{\text{min}}^-$	$z^+ = z_{\text{max}}^+$	$z = 0$	$U_{\text{min}}$ [V]	2.0	2.8

Table 2: Upper and lower cutoff potential specified for each electrode chemistry used in this work.

Figures 1b to 1e illustrate how  $U_{\text{OCV}}(z)$  is assembled from  $U_{\text{OCP}}^\pm(z^\pm)$  and depends on  $r_{\text{N/P}}$  and  $z_0^+$  (see figure 3 in the Supporting Information for an illustration of such OCV assembly using conventional line plots). In this work, we will use the LFP/ and NMC (lithium nickel manganese cobalt oxide)/graphite cell chemistry as two typical running examples and perform simulations coded in Python to concretely illustrate our results, where the electrode OCP relations are from the LFP, NMC-111 and MCMB (mesocarbon microbeads, a form of synthetic graphite) OCP fits provided in Plett [4, sec. 3.11.1], with temperature set to 25°C. However, our results apply equally to all other chemistries. The specifications of electrode cutoff potential and full-cell cutoff voltage are tabulated in tables 1 and 2, respectively.

In fig. 1b inspired by Olson et al. [9], each line segment corresponds to a cell’s  $z^+(z^-)$  relation with a particular  $(r_{\text{N/P}}, z_0^+)$  pair, where the N/P ratio  $r_{\text{N/P}}$  is the negative slope and the Li/P ratio  $z_0^+$  (recall eq. (8)) is the  $z^+$ -axis intercept. The four pairs of N/P and Li/P ratio other than  $r_{\text{N/P}} = z_0^+ = 1$  cover the four characteristic regimes to be discussed in section 2.7. These line segments are superposed on the 2D landscape of  $U_{\text{OCV}}(z^-, z^+)$ . The  $U_{\text{min}}$ -contour marks where these segments can start on the top left, while the  $U_{\text{max}}$ -contour marks their possible ends on the bottom right. Then the slope  $-r_{\text{N/P}}$  and intercept  $z_0^+$  determine whether the segment starts close to the top or left side of the square, and whether it ends near the bottom or right side. Therefore, this indicates the electrode SOC limits at the fully discharged and charged state, which implies which electrode is more limiting towards the end of discharging and charging, as will be further discussed in section 2.4. When we plot the OCV profile intersected by each line segment and scale the segment to a unit interval, we obtain the  $z$ -based OCV  $U_{\text{OCV}}(z)$  in fig. 1d. The flatness of the LFP and MCMB OCP makes the variation in  $U_{\text{OCV}}(z)$  rather mild visually with different  $(r_{\text{N/P}}, z_0^+)$  pairs, which will be precisely quantified in sections 2.5 and 3.1. Figures 1c and 1e are simply the NMC/MCMB counterparts of figs. 1b and 1d. The steeper slope of the NMC OCP curve is reflected by the narrower contour spacing in fig. 1c and the larger variation between different OCV curves in fig. 1e.

One advantage of the  $z$ -based OCV  $U_{\text{OCV}}(z)$  is that it can be determined directly by full-cell

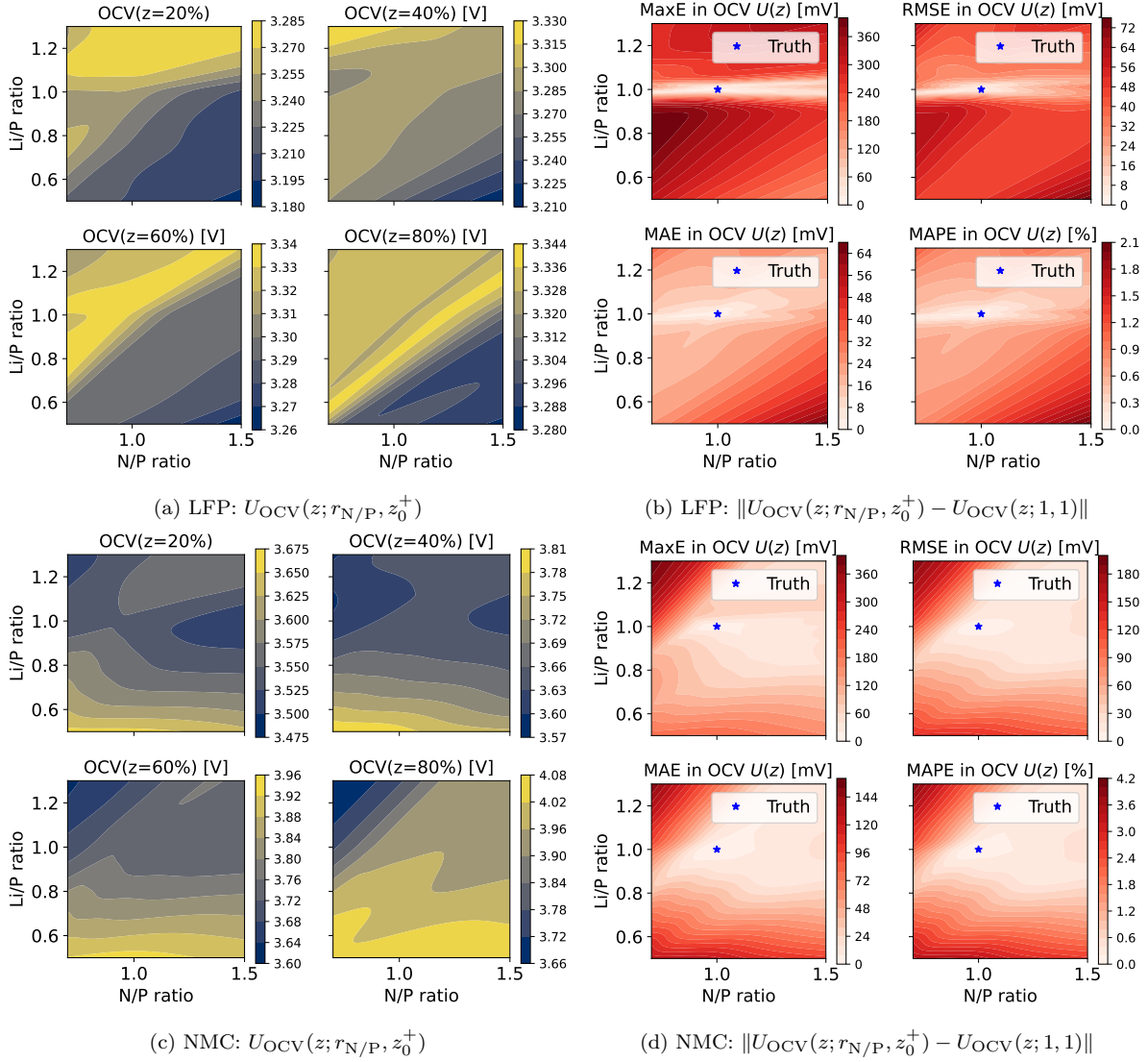


Figure 2: **(a, b)** LFP/MCMB. **(c, d)** NMC/MCMB. **(a, c)** Cell OCV at SOC  $z = 20\%$ ,  $40\%$ ,  $60\%$ , and  $80\%$  with different  $(r_{N/P}, z_0^+)$  pairs. Note the varied OCV sensitivity at different  $z$ 's. **(b, d)** Maximum errors (MaxE), Root-mean-square errors (RMSE), mean absolute errors (MAE), and mean absolute percentage errors (MAPE) between cell OCV with an arbitrary  $(r_{N/P}, z_0^+)$  pair and OCV with  $r_{N/P} = 1$  and  $z_0^+ = 1$  (marked as truth).

measurements without knowing anything about electrode OCP and SOC, just as how  $U_{\text{OCP}}^{\pm}(z^{\pm})$  can be determined agnostic of stoichiometry  $x^{\pm}$ . Moreover, this function can be roughly assumed unchanged upon aging [6] because by definition,  $U_{\text{OCV}}(z)$  always monotonically increases from  $(0, U_{\text{min}})$  to  $(1, U_{\text{max}})$ , as figs. 1d and 1e illustrate. Hence, such electrode-agnostic monolithic cell OCV has been used in most ECMs in literature and in prevailing battery management systems [4, 5]. However, previous literature and the above have shown that  $U_{\text{OCV}}(z)$  does change appreciably upon aging, as further corroborated by fig. 2 based on simulations. Figures 2a and 2c show how  $U_{\text{OCV}}(z)$  at a particular  $z$  varies with the Li/P and N/P ratio ranging in  $[0.5, 1.3]$  and  $[0.7, 1.5]$ , respectively. The OCV variation is between 60 mV and 100 mV at these SOC for LFP, while it is as large as 200 mV to 400 mV for NMC.

Note that in a typical commercial lithium-ion cell, the NE is manufactured as fully delithiated, while the PE as fully lithiated, so upon formation cycles, after some lithium is consumed to form the SEI (solid-electrolyte interface) layers, we should expect the Li/P ratio to be less than 1. Moreover, when graphite is used as the NE, to avoid lithium plating and other side reactions during charging, we typically design the N/P ratio to be slightly larger than 1. However, when a cell degrades upon cycling or storage, lithium inventory and active materials may not diminish at the same rate so the N/P and Li/P ratio can potentially evolve to other non-typical values. This is why in this work, we study the cell OCV characteristics across a large range of these two parameters to provide a big picture of a cell's potential behaviors throughout its life.

If we summarize the difference between two complete OCV curve  $U_{\text{OCV}}(z)$  by a norm, and compare the  $U_{\text{OCV}}(z)$  of different  $(r_{\text{N/P}}, z_0^+)$  pairs to the one with a fixed pair considered as the ground truth, we obtain figs. 2b and 2d. For the LFP case in fig. 2b, note in certain regions, RMSE and especially MaxE are much higher than MAE, implying that the errors between two OCV curves are distributed very unevenly along  $z$ , so only OCV values within certain SOC windows are informative about the parameters. It is also evident in this case that the OCV is much more sensitive to Li/P than to N/P. In summary, these results indicate that the OCV variation does encode changes in  $r_{\text{N/P}}$  and  $z_0^+$  and hence changes in degradation modes, although the sensitivity can be highly chemistry-dependent and vary across different  $(r_{\text{N/P}}, z_0^+)$  pairs.

The upper and lower cutoff voltage also define the cell total capacity  $\hat{Q}_{\text{max}}$ , which is the charge throughput associated with the SOC interval  $0 \leq z \leq 1$ . The electrode SOC limits in (11) also relate the electrode capacity to their full-cell counterpart by charge conservation:

$$\hat{Q}_{\text{max}} = (z_{\text{max}}^- - z_{\text{min}}^-)\hat{Q}_{\text{max}}^- = (z_{\text{max}}^+ - z_{\text{min}}^+)\hat{Q}_{\text{max}}^+. \quad (13)$$

We have already mentioned that the four electrode SOC limits are parametrized by  $r_{\text{N/P}}$  and  $z_0^+$  only, so  $\hat{Q}_{\text{max}}$  also depends on these two dimensionless quantities, but is additionally parametrized by the dimensional  $\hat{Q}_{\text{max}}^+$ . Of course  $\hat{Q}_{\text{max}}^+$  is not the only choice, we choose it here for symmetry since it is the denominator of both  $r_{\text{N/P}}$  and  $z_0^+$ . Equivalently,  $\hat{Q}_{\text{max}}$  can also be parametrized by the three-dimensional SOH parameter  $\hat{Q}_{\text{max}}^{\text{Li}}$ ,  $\hat{Q}_{\text{max}}^-$ , and  $\hat{Q}_{\text{max}}^+$ . We will discuss the trade-off between these two options.

Since what Coulomb counting records is the charge or discharge throughput, sometimes we also want to express cell OCV in terms of, say charge throughput  $\hat{Q}$ , instead of the dimensionless SOC  $z$ . Assume  $\hat{Q}$  counts from the fully discharged state at  $U_{\text{min}}$ , we readily have  $z = \hat{Q}/\hat{Q}_{\text{max}}$  and it ultimately yields

$$U_{\text{OCV}}(\hat{Q}) = U_{\text{OCP}}^+(z_{\text{max}}^+ - \hat{Q}/\hat{Q}_{\text{max}}^+) - U_{\text{OCP}}^-(z_{\text{min}}^- + \hat{Q}/\hat{Q}_{\text{max}}^-), \quad (14)$$

which is essentially the same as (4) used by [11], except that  $U_{\text{OCV}}(\hat{Q})$  under our formulation here

are parametrized by three independent SOH parameters  $r_{\text{N/P}}$ ,  $z_0^+$ , and  $\hat{Q}_{\text{max}}^+$ , or equivalently by  $\hat{Q}_{\text{max}}^{\text{Li}}$  and  $\hat{Q}_{\text{max}}^\pm$ , neither of which depends on the choice of cell cutoff voltage  $U_{\text{max}}$  or  $U_{\text{min}}$ .

The cutoff-voltage independence also makes (14) easily adaptable to modelling partial OCV curve. If the starting voltage  $U_{\text{start}}$  is known (e.g., reliably measured after a long rest), the initial electrode SOC  $z_{\text{start}}^\pm$  are uniquely determined by  $U_{\text{start}}$  and any three-parameter set above, so after substituting  $z_{\text{start}}^\pm$  into  $z^{\text{+max}}$  and  $z_{\text{min}}^-$  in (14), this partial OCV model is still parametrized by the same three parameters. However, if  $U_{\text{start}}$  is subject to the same uncertainty as any subsequent OCV measurements are, we will have to add an extra unknown parameter, such as  $z_{\text{start}}^-$ , to mark the electrode SOC to be matched with the beginning of the partial OCV. One popular parametrization for this case in literature is with  $z_{\text{start}}^\pm$  and  $\hat{Q}_{\text{max}}^\pm$  [18]. Although it is mathematically equivalent to using  $z_{\text{start}}^-$ ,  $\hat{Q}_{\text{max}}^{\text{Li}}$  and  $\hat{Q}_{\text{max}}^\pm$ , the physical meaning of each parameter in the latter might be clearer and more intuitive.

In the above analysis, we have assumed no LLI or LAM during charging or discharging. In practice, due to the slowness of degradation compared to charging and discharging, this assumption is valid within a few cycles so the above OCV model will be a good approximation, and we only need to gradually adjust the SOH parameters upon cell aging.

### 2.3. Relating SOH Parameters to LLI and LAM Percentage

We have parametrized  $U_{\text{OCV}}(z)$  by the dimensionless N/P ratio  $r_{\text{N/P}}$  and Li/P ratio  $z_0^+$ , and parametrized  $U_{\text{OCV}}(\hat{Q})$  by the dimensional lithium inventory  $\hat{Q}_{\text{max}}^{\text{Li}}$  and PE and NE active material capacity  $\hat{Q}_{\text{max}}^\pm$ . All these SOH parameters are independent of cell cutoff voltage and agnostic of the pristine-cell condition.

In cases where we can specify the initial lithium inventory and active material amount in a pristine cell, denoted by  $\hat{Q}_{\text{max,ini}}^{\text{Li}}$  and  $\hat{Q}_{\text{max,ini}}^\pm$ , respectively, we can easily calculate the commonly used LLI, LAMn, and LAMp percentage as derived quantities:

$$\text{LLI} = 1 - \frac{\hat{Q}_{\text{max}}^{\text{Li}}}{\hat{Q}_{\text{max,ini}}^{\text{Li}}}, \quad \text{LAM}^- = 1 - \frac{\hat{Q}_{\text{max}}^-}{\hat{Q}_{\text{max,ini}}^-}, \quad \text{LAM}^+ = 1 - \frac{\hat{Q}_{\text{max}}^+}{\hat{Q}_{\text{max,ini}}^+}. \quad (15)$$

We can similarly correlate the N/P ratio  $r_{\text{N/P}}$  and Li/P ratio  $z_0^+$  to their initial values:

$$r_{\text{N/P}} = r_{\text{N/P,ini}} \frac{1 - \text{LAM}^-}{1 - \text{LAM}^+}, \quad z_0^+ = z_{0,\text{ini}}^+ \frac{1 - \text{LLI}}{1 - \text{LAM}^+}, \quad (16)$$

as similarly shown by, for example, equation (5) and (8') in [8] and equation (48-49) in [9].

In literature, it is not uncommon to see parametric study of an OCV model by varying the above three loss percentages, but this has the caveat of redundancy, because as we have shown, the shape of an OCV curve, or the SOC-based OCV, is only governed by two degrees of freedom, i.e., the N/P and Li/P ratio. The issue here is that a certain ratio  $\text{LLI} : \text{LAM}^- : \text{LAM}^+$  does not correspond to a unique shape of OCV, which gives the false impression that the OCV variation has more than two degrees of freedom. Indeed, it is the ratio  $(1 - \text{LLI}) : (1 - \text{LAM}^-) : (1 - \text{LAM}^+)$ , which corresponds to a fixed ratio of  $\hat{Q}_{\text{max}}^{\text{Li}} : \hat{Q}_{\text{max}}^- : \hat{Q}_{\text{max}}^+$  according to (15) and hence fixed N/P and Li/P ratio, that will uniquely determine the OCV shape. Of course, if a dimensional charge-based coordinate must be used in place of the dimensionless cell SOC  $z$  when, for example,  $z$  is not accessible in certain practical scenarios, the OCV curve will depend on all three parameters of  $\hat{Q}_{\text{max}}^{\text{Li}}$  and  $\hat{Q}_{\text{max}}^\pm$ , which can now be equivalently re-parametrized by LLI and  $\text{LAM}^\pm$  instead.

Another subtlety already alluded to in section 2.1 lies in the dependence of the SOH parameters  $\hat{Q}_{\text{max}}^{\text{Li}}$  and  $\hat{Q}_{\text{max}}^\pm$  on the artificial choice of electrode cutoff potential. For the active materials, the

situation is relatively straightforward, because when we change the upper and lower cutoff potential, it simply changes the stoichiometry range considered usable, and thus  $\hat{Q}_{\max}^{\pm}$  are just scaled by the same factor as the length of the stoichiometry range is. For LAM percentage calculation, since both the initial and current active materials are scaled the same way, LAM $^{\pm}$  will remain the same.

Things are more complicated for lithium inventory [21]. Since we essentially set some lower limit of stoichiometry corresponding to some upper cutoff potential as the “origin” of counting lithium (recall eq. (8)), changing the upper cutoff potential will alter the lithium inventory but changing the lower one will not, because only the former is relevant to the origin. Moreover, since this origin only affects  $\hat{Q}_{\max}^{\text{Li}}$  itself but not its change, LLI will also depend on this choice of lithium origin.

Since all of  $\hat{Q}_{\max}^{\text{Li}}$  and  $\hat{Q}_{\max}^{\pm}$  depend on the choice of electrode cutoff potentials, the N/P ratio  $r_{\text{N/P}}$  and Li/P ratio  $z_0^+$  will also vary inevitably. However, when assembling the full-cell OCV, as long as the full-cell cutoff voltages remain the same, the SOC-based OCV  $U_{\text{OCV}}(z)$  also remains constant, because we are simply renaming the electrode SOC at the cell cutoff voltages without altering what electrode potentials they correspond to. Consequently, the total capacity within this voltage window is also unaffected. Furthermore, the same N/P and Li/P ratio will still uniquely determine  $U_{\text{OCV}}(z)$ .

Although defining the electrode SOC based on specifying some material-specific cutoff potential seems to introduce certain arbitrariness, a reasonable choice is usually available, and it does make the SOH parameters  $\hat{Q}_{\max}^{\text{Li}}$  and  $\hat{Q}_{\max}^{\pm}$  more relevant to practical operation. Moreover, data under one choice of electrode cutoff potentials can easily be transformed into their counterparts under another choice as post-processing. Therefore, as long as we keep the choice consistent and explicitly report it when discussing these SOH parameters, the use of electrode SOC should do more benefit than harm.

#### 2.4. Parametric Sensitivity: Electrode DV Fraction and Role of Fixed Cutoff Voltage

We first establish sensitivity results for a general parameter  $\alpha$  of an electrode-specific cell OCV model  $U_{\text{OCV}}(z)$ , which will then be applied to various specific SOH parameters. For the most general case, any input functional relation to eq. (12) that must be specified might depend on  $\alpha$ :

$$U_{\text{OCP}}^+(z^+, \alpha), \quad U_{\text{OCP}}^-(z^-, \alpha), \quad z^+(z^-, \alpha), \quad (17)$$

which together constitute the final  $U_{\text{OCV}}(z, \alpha)$ .

By the chain rule, we have (derivation details in Supporting Information)

$$\begin{aligned} \partial_{\alpha} U_{\text{OCV}}(z) &= \partial_{\alpha} U_{\text{OCP}}^+(z^+) + d_{z^+} U_{\text{OCP}}^+ \cdot \partial_{\alpha} z^+(z) \\ &\quad - \partial_{\alpha} U_{\text{OCP}}^-(z^-) - d_{z^-} U_{\text{OCP}}^- \cdot \partial_{\alpha} z^-(z), \end{aligned} \quad (18)$$

$$\partial_{\alpha} z^+(z) = \partial_{\alpha} z^+(z^-) - r_{\text{N/P}} \partial_{\alpha} z^-(z), \quad (19)$$

$$\partial_{\alpha} z^-(z) = (1 - z) \partial_{\alpha} z_{\min}^- + z \partial_{\alpha} z_{\max}^-. \quad (20)$$

$$\partial_{\alpha} z^-(U_{\text{OCV}}) = \frac{\partial_{\alpha} U_{\text{OCP}}^+(z^+) + d_{z^+} U_{\text{OCP}}^+ \cdot \partial_{\alpha} z^+(z^-) - \partial_{\alpha} U_{\text{OCP}}^-(z^-)}{r_{\text{N/P}} d_{z^+} U_{\text{OCP}}^+ + d_{z^-} U_{\text{OCP}}^-}. \quad (21)$$

$$\partial_{\alpha} z_{\min}^- = \partial_{\alpha} z^-(U_{\min}), \quad \partial_{\alpha} z_{\max}^- = \partial_{\alpha} z^-(U_{\max}). \quad (22)$$

Note that we denote parametric partial derivatives by  $\partial_{\alpha}$  while all the other state partial differentiation by  $d_{(\cdot)}$  to emphasize the distinction. One subtlety here is that  $z_{\min}^-$  is defined implicitly by the lower cutoff voltage as  $U_{\text{OCV}}(z_{\min}^-) = U_{\min}$ . Therefore, calculating  $\partial_{\alpha} z_{\min}^-$  reduces to differentiating the implicit function  $z^-(U_{\text{OCV}}, \alpha)$  defined by  $U_{\text{OCV}}(z^-, \alpha)$ .

Since generically, we have  $\partial_\alpha z^\pm(z) \neq 0$ , the change of  $\alpha$  may cause the same  $z$  to correspond to a different  $z^\pm$ . In particular, the electrode SOC limits  $z_{\min}^-$ ,  $z_{\max}^-$ ,  $z_{\min}^+$ , and  $z_{\max}^+$  at the upper and lower cutoff voltage can change with  $\alpha$ , causing the “charge/discharge end-point slippage” [22, 23]. In contrast, the PE-NE relative slippage indicated by  $\partial_\alpha z^+(z^-) \neq 0$  causing one  $z^-$  to correspond to a different  $z^+$  will also occur unless both  $r_{N/P}$  and  $z_0^+$  are fixed, i.e. the ratio  $\hat{Q}_{\max}^- : \hat{Q}_{\max}^+ : \hat{Q}_{\max}^{\text{Li}}$  stays the same. A lot of researchers have studied such electrode slippage due to SEI growth during charging, but what we have derived above reveal a bigger picture of other potential underlying mechanisms.

The  $z^-(z)$  and  $z^+(z)$  slippage also causes the electrode potential  $U_{\text{OCP}}^\pm(z^\pm(z))$  and consequently the cell OCV  $U_{\text{OCV}}(z)$  to change for a particular  $z$ . Therefore, a certain cell SOC  $z$  does not anchor to any electrode SOC  $z^\pm$  or any OCV value (except for  $z = 0$  and  $z = 1$  in the latter case). The cell SOC  $z$  simply indicates the relative remaining discharge throughput against total capacity  $\hat{Q}_{\max}$  until fully discharged. This is probably the only persistent physical meaning of a so-defined cell SOC  $z$ .

In addition to the cell OCV  $U_{\text{OCV}}(z)$  that is independent of the total capacity, we can also characterize the parametric sensitivity of total capacity  $\hat{Q}_{\max} = (z_{\max}^- - z_{\min}^-)\hat{Q}_{\max}^-$  by

$$\partial_\alpha \hat{Q}_{\max} = (\partial_\alpha z_{\max}^- - \partial_\alpha z_{\min}^-)\hat{Q}_{\max}^- + (z_{\max}^- - z_{\min}^-)\partial_\alpha \hat{Q}_{\max}^-. \quad (23)$$

Any particular parameter will usually not appear in all three functional relations in (17), which will thus simplify eqs. (18) to (22). There are two main types of such cases. The first type is a parameter that only affects the two electrode OCP relations but not  $z^+(z^-)$ , such as temperature [4] or parameters governing the component changes in composite electrode active materials [24] if they do not also affect the electrode capacity. In this case, eqs. (19) and (21) reduce to

$$\partial_\alpha z^+(z) = -r_{N/P}\partial_\alpha z^-(z), \quad (24)$$

$$\partial_\alpha z^-(U_{\text{OCV}}) = \frac{\partial_\alpha U_{\text{OCP}}^+(z^+) - \partial_\alpha U_{\text{OCP}}^-(z^-)}{r_{N/P}d_{z^+}U_{\text{OCP}}^+ + d_{z^-}U_{\text{OCP}}^-}. \quad (25)$$

We will not look into this type of parameters in this work.

The other type includes  $r_{N/P}$  and  $z_0^+$  or their re-parametrization, which are related to LLI and LAM and affect only  $z^+(z^-)$  but not the electrode OCP. In this case, eqs. (18) and (21) reduce to:

$$\partial_\alpha U_{\text{OCV}}(z) = d_{z^+}U_{\text{OCP}}^+ \cdot \partial_\alpha z^+(z) - d_{z^-}U_{\text{OCP}}^- \cdot \partial_\alpha z^-(z), \quad (26)$$

$$\partial_\alpha z^-(U_{\text{OCV}}) = \frac{d_{z^+}U_{\text{OCP}}^+}{r_{N/P}d_{z^+}U_{\text{OCP}}^+ + d_{z^-}U_{\text{OCP}}^-} \partial_\alpha z^+(z^-). \quad (27)$$

The physical meaning of the apparently complicated fraction coefficient in (27) can be revealed by defining the dimensional counterparts of the electrode and cell SOC as

$$\hat{Q}^\pm = z^\pm \hat{Q}_{\max}^\pm, \quad \hat{Q} = z \hat{Q}_{\max}, \quad (28)$$

and with charge conservation  $d\hat{Q} = d\hat{Q}^- = -d\hat{Q}^+$ , rewriting the fraction as

$$\frac{1}{r_{N/P}} \frac{r_{N/P}d_{z^+}U_{\text{OCP}}^+}{r_{N/P}d_{z^+}U_{\text{OCP}}^+ + d_{z^-}U_{\text{OCP}}^-} = \frac{1}{r_{N/P}} \frac{d_{\hat{Q}^+}U_{\text{OCP}}^+}{d_{\hat{Q}^+}U_{\text{OCP}}^+ + d_{\hat{Q}^-}U_{\text{OCP}}^-} = \frac{1}{r_{N/P}} \frac{d_{\hat{Q}}U_{\text{OCP}}^+}{d_{\hat{Q}}U_{\text{OCV}}}.$$

Since  $d_{\hat{Q}^+}U_{\text{OCP}}^+$  and  $d_{\hat{Q}^-}U_{\text{OCP}}^-$  are both negative, the second fraction factor above can be interpreted as the fraction of the PE contribution to the full-cell differential voltage.

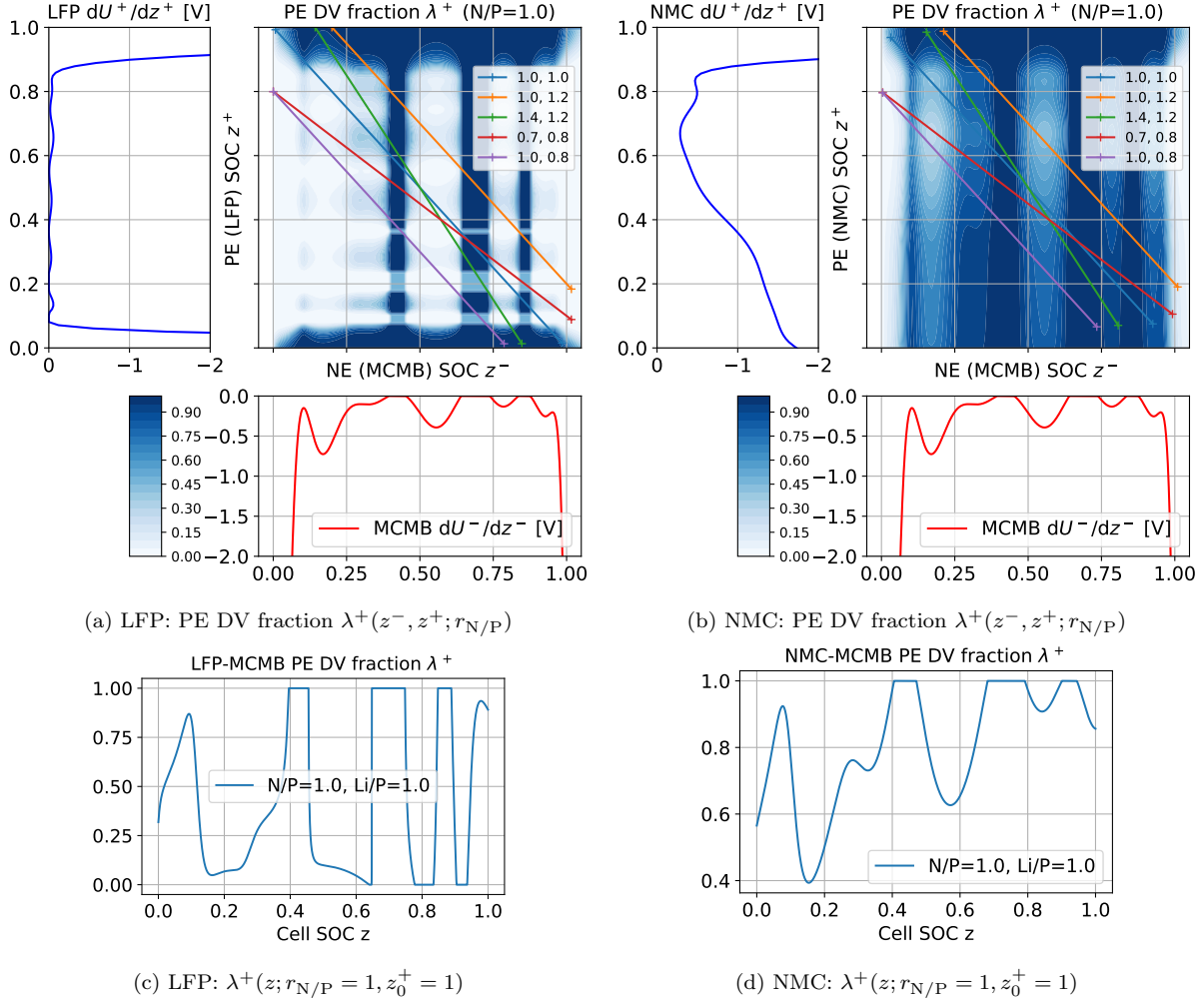


Figure 3: **(a)** PE DV fraction square plots (inspired by but different from the DV square plots of Olson et al. [9]) of the LFP-MCMB chemistry overlaid with five lines of  $z^+(z^-)$  corresponding to cells with different  $(r_{N/P}, z_0^+)$  pairs as indicated by the legends. Note that the color bar is associated with the contours. Such plots can be read analogously to how the OCV square plots Figs. 1b and 1c are interpreted. **(c)** The PE DV fraction with  $(r_{N/P} = 1, z_0^+ = 1)$ . This can again be read off from (a), where the peaks and troughs correspond to where the blue line in (a) crosses the dark and light areas, respectively. **(b, d)** NMC/MCMB counterparts of (a, c).



Due to the important role played by this fraction in subsequent sensitivity gradients and its clear physical meaning, we call it the PE DV (differential voltage) fraction and denote it by

$$\lambda^+ = \frac{r_{\text{N/P}} d_{z^+} U_{\text{OCP}}^+}{r_{\text{N/P}} d_{z^+} U_{\text{OCP}}^+ + d_{z^-} U_{\text{OCP}}^-} = \frac{d_{\hat{Q}^+} U_{\text{OCP}}^+}{d_{\hat{Q}^+} U_{\text{OCP}}^+ + d_{\hat{Q}^-} U_{\text{OCP}}^-} \in [0, 1] \quad (29)$$

and the NE DV fraction is simply  $\lambda^- = 1 - \lambda^+$ . Figures 3a and 3c show  $\lambda^+(z^-, z^+)$  and how  $\lambda^+(z)$  is obtained analogously to how  $U_{\text{OCV}}(z)$  is obtained from  $U_{\text{OCV}}(z^-, z^+)$  in figs. 1b and 1d. Note that compared to  $U_{\text{OCV}}(z^-, z^+)$ , which is independent of  $r_{\text{N/P}}$  or  $z_0^+$ ,  $\lambda^+(z^-, z^+)$  as defined by 29 does depend on  $r_{\text{N/P}}$ , although empirically this dependence is weak and does not alter the overall pattern of  $\lambda^+(z^-, z^+)$ . Therefore, we still overlay the  $\lambda^+$  landscape at  $r_{\text{N/P}} = 1$  in fig. 3a with segments of different  $(r_{\text{N/P}}, z_0^+)$  pairs for illustration purpose.

Since in eq. (20), we only need the PE DV fraction (27) at the lower and upper cutoff voltage, we specifically define

$$\lambda_{\text{l}}^+ = \frac{r_{\text{N/P}} d_{z^+} U_{\text{OCP}}^+|_{z_{\text{max}}^+}}{r_{\text{N/P}} d_{z^+} U_{\text{OCP}}^+|_{z_{\text{max}}^+} + d_{z^-} U_{\text{OCP}}^-|_{z_{\text{min}}^-}}, \quad \lambda_{\text{u}}^+ = \frac{r_{\text{N/P}} d_{z^+} U_{\text{OCP}}^+|_{z_{\text{min}}^+}}{r_{\text{N/P}} d_{z^+} U_{\text{OCP}}^+|_{z_{\text{min}}^+} + d_{z^-} U_{\text{OCP}}^-|_{z_{\text{max}}^-}} \quad (30)$$

associated with  $U_{\text{min}}$  and  $U_{\text{max}}$ , respectively. The above also implies that the sole reason why the electrode DV fractions play a role in our sensitivity analysis is the dependence of cell SOC  $z$  and total capacity  $\hat{Q}_{\text{max}}$  on the artificially specified lower and upper cutoff voltage.

The PE DV fraction  $\lambda_{\text{u}}^+$  and  $\lambda_{\text{l}}^+$  also quantify to what extent each electrode limits the charging or discharging towards the respective cutoff voltage, which has been studied in the context of discerning Coulombic efficiency and capacity retention [25, 23]. Note that the  $\lambda$  defined in [23] is just  $\lambda_{\text{l}}^+$  here, while their  $\omega$  is essentially  $(\lambda_{\text{u}}^+ - 1)$ . We follow their notations to denote the PE DV fraction by letter  $\lambda$ , while the definition of  $\omega$  seems to introduce an extra unnecessary quantity seemingly different from  $\lambda$ , which shadows the structural symmetry between NE and PE, and whose negative sign also makes its interpretation less straightforward.

When  $\lambda_{\text{l}}^+ \approx 1$ , it implies that the cell reaches  $U_{\text{min}}$  in discharging mainly due to the sharp drop of  $U^+(z^+)$  rather than the steep increase of  $U^-(z^-)$ , mostly caused by PE getting filled up with  $\text{Li}^+$  due to  $\hat{Q}_{\text{max}}^{\text{Li}} > \hat{Q}_{\text{max}}^+$ , or equivalently  $z_0^+ > 1$ . This gives rise to PE-limited discharging. In contrast, when  $\lambda_{\text{l}}^+ \approx 0$ , the cell reaches  $U_{\text{min}}$  mostly due to the  $\text{Li}^+$  depletion in the NE and thus the steep rise of its potential, hence called NE-limited discharging. We can likewise define PE- and NE-limited charging. Figure 4 illustrates how the electrode SOC limits and PE DV fractions vary with the N/P ratio  $r_{\text{N/P}}$  and Li/P ratio  $z_0^+$ , which can be divided into four quadrants depending on whether  $z_0^+ > 1$  and  $z_0^+ > r_{\text{N/P}}$ , or more intuitively, whether  $\hat{Q}_{\text{max}}^{\text{Li}} > \hat{Q}_{\text{max}}^+$  and  $\hat{Q}_{\text{max}}^{\text{Li}} > \hat{Q}_{\text{max}}^-$ . The NMC case has a more gradual transition across these regimes than the LFP case. We will go into more depth concerning these four regimes in sections 2.6 and 2.7.

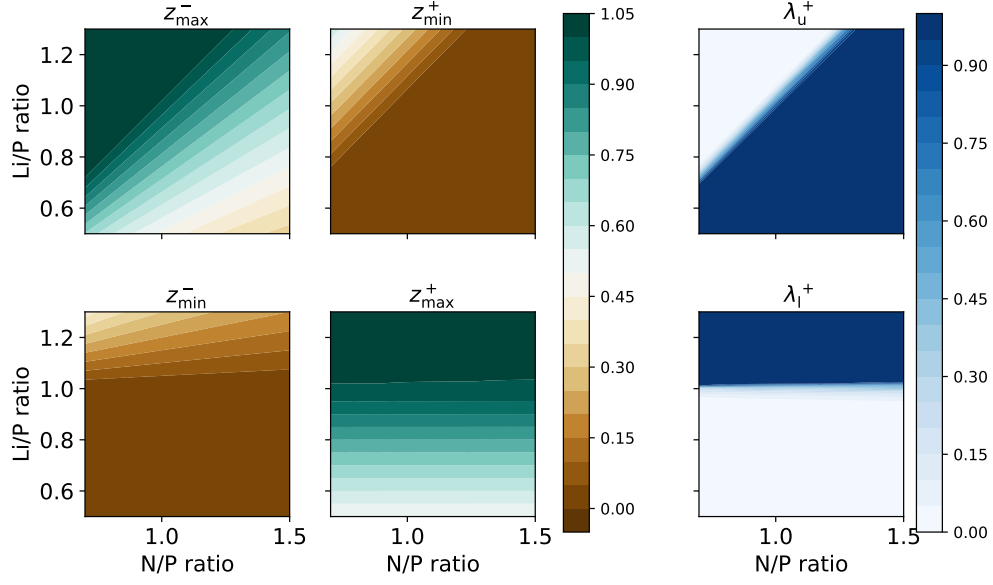
With the introduction of the PE DV fraction  $\lambda^+$ , eq. (22) simplifies to

$$\partial_{\alpha} z_{\text{min}}^- = \frac{\lambda_{\text{l}}^+}{r_{\text{N/P}}} \partial_{\alpha} z^+(z_{\text{min}}^-), \quad \partial_{\alpha} z_{\text{max}}^- = \frac{\lambda_{\text{u}}^+}{r_{\text{N/P}}} \partial_{\alpha} z^+(z_{\text{max}}^-), \quad (31)$$

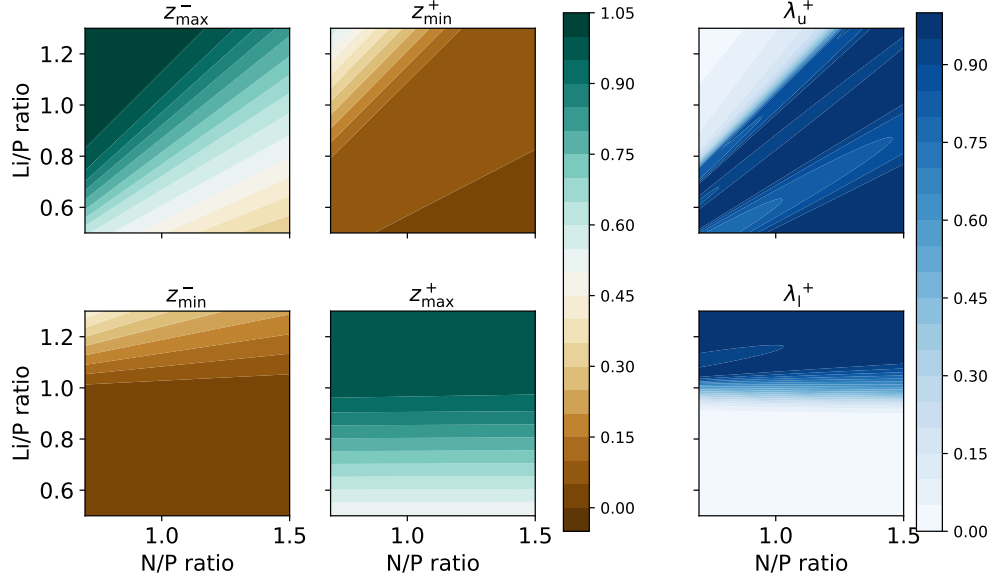
which paves the way for deriving the sensitivity gradients with respect to  $r_{\text{N/P}}$  and  $z_0^+$ .

## 2.5. SOH-Sensitivity Gradients of Electrode SOC Limits and Cell OCV

Before proceeding, we must point out a subtlety omitted in previous parts. A partial derivative with respect to a particular parameter  $\alpha$  itself is ambiguous, because it also depends on the complete



(a) LFP/MCMB



(b) NMC/MCMB

Figure 4: Electrode SOC limits (**left**) and PE DV fractions (**right**) at different N/P ratio and Li/P ratio. In either (a) or (b), the top regards the fully charged state  $U_{OCV} = U_{max}$ , where the variation mostly depends on  $z_0^+/r_{N/P}$ , which is essentially the Li/N ratio, and has a sharp change at  $z_0^+/r_{N/P} = 1$ . In contrast, the bottom is at the fully discharged state  $U_{OCV} = U_{min}$ , whose variation mostly depends on the Li/P ratio and has a sharp change at  $z_0^+ = 1$ .

parametrization, i.e. choices of parameters other than  $\alpha$ . All the previous results still hold, but we must specify the full set of parameters before carrying out concrete calculations.

We know that  $U_{\text{OCV}}(z)$  can be parametrized by  $r_{\text{N/P}}$  and  $z_0^+$ , so  $(r_{\text{N/P}}, z_0^+)$  serves as the complete parameter set for the following partial differentiation. From eq. (7), we can easily obtain

$$\partial_{r_{\text{N/P}}} z^+(z^-) = -z^-, \quad \partial_{z_0^+} z^+(z^-) = 1. \quad (32)$$

We first derive the counterparts of eqs. (18) to (22) for  $r_{\text{N/P}}$ :

$$\frac{\partial z^-(U_{\text{OCV}})}{\partial r_{\text{N/P}}} = \left. \frac{-z^-\lambda^+}{r_{\text{N/P}}} \right|_{U_{\text{OCV}}}, \quad (33)$$

$$\frac{\partial z_{\text{min}}^-}{\partial r_{\text{N/P}}} = \frac{-z_{\text{min}}^-\lambda_{\text{l}}^+}{r_{\text{N/P}}}, \quad \frac{\partial z_{\text{max}}^-}{\partial r_{\text{N/P}}} = \frac{-z_{\text{max}}^-\lambda_{\text{u}}^+}{r_{\text{N/P}}}, \quad (34)$$

$$\frac{\partial z^-(z)}{\partial r_{\text{N/P}}} = -\frac{(1-z)z_{\text{min}}^-\lambda_{\text{l}}^+ + zz_{\text{max}}^-\lambda_{\text{u}}^+}{r_{\text{N/P}}}, \quad \frac{\partial z^+(z)}{\partial r_{\text{N/P}}} = -(1-z)z_{\text{min}}^-\lambda_{\text{l}}^- - zz_{\text{max}}^-\lambda_{\text{u}}^-, \quad (35)$$

$$\frac{\partial U_{\text{OCV}}(z)}{\partial r_{\text{N/P}}} = \frac{dU_{\text{OCP}}^+}{dz^+} \frac{\partial z^+(z)}{\partial r_{\text{N/P}}} - \frac{dU_{\text{OCP}}^-}{dz^-} \frac{\partial z^-(z)}{\partial r_{\text{N/P}}}. \quad (36)$$

As we can see, both  $\partial_{r_{\text{N/P}}} z^\pm(z)$  vary linearly with  $z$ , which is not surprising since  $z^\pm(z)$  have to remain linear by definition of  $z$ .

Figure 5 demonstrates empirically how the  $z^-$ -based OCV  $U_{\text{OCV}}(z^-)$  and  $z$ -based OCV  $U_{\text{OCV}}(z)$  vary with the N/P ratio  $r_{\text{N/P}}$  on the top, and the  $r_{\text{N/P}}$ -derivatives  $\partial_{r_{\text{N/P}}} z^\pm(z)$ ,  $\partial_{r_{\text{N/P}}} U_{\text{OCP}}^\pm(z)$ , and  $\partial_{r_{\text{N/P}}} U_{\text{OCV}}(z)$  evaluated at  $r_{\text{N/P}} = 1$ . Figure 5a shows that  $z_{\text{max}}^-$  quickly decreases with increasing  $r_{\text{N/P}}$ , while  $z_{\text{min}}^-$  is insensitive to  $r_{\text{N/P}}$  in this case, which is consistent with  $\partial_{r_{\text{N/P}}} z^-(z=1) < -0.8$  and  $\partial_{r_{\text{N/P}}} z^-(z=0) \approx 0$  as indicated by fig. 5c. On the other hand, due to the OCP curves in both electrodes being rather flat for a large mid-SOC range,  $U_{\text{OCV}}(z)$  is not very sensitive to  $r_{\text{N/P}}$  overall (fig. 5b) and the several narrow SOC windows with relatively high sensitivity are also aligned with what the  $r_{\text{N/P}}$ -derivatives imply in fig. 5d.

Next, we carry out the same sensitivity analysis with respect to  $z_0^+$ :

$$\frac{\partial z^-(U_{\text{OCV}})}{\partial z_0^+} = \left. \frac{\lambda^+}{r_{\text{N/P}}} \right|_{U_{\text{OCV}}}, \quad (37)$$

$$\frac{\partial z_{\text{min}}^-}{\partial z_0^+} = \frac{\lambda_{\text{l}}^+}{r_{\text{N/P}}}, \quad \frac{\partial z_{\text{max}}^-}{\partial z_0^+} = \frac{\lambda_{\text{u}}^+}{r_{\text{N/P}}}, \quad (38)$$

$$\frac{\partial z^-(z)}{\partial z_0^+} = \frac{(1-z)\lambda_{\text{l}}^+ + z\lambda_{\text{u}}^+}{r_{\text{N/P}}}, \quad \frac{\partial z^+(z)}{\partial z_0^+} = (1-z)\lambda_{\text{l}}^- + z\lambda_{\text{u}}^-, \quad (39)$$

$$\frac{\partial U_{\text{OCV}}(z)}{\partial z_0^+} = \frac{dU_{\text{OCP}}^+}{dz^+} \frac{\partial z^+(z)}{\partial z_0^+} - \frac{dU_{\text{OCP}}^-}{dz^-} \frac{\partial z^-(z)}{\partial z_0^+}. \quad (40)$$

Again, fig. 6, which is the  $z_0^+$ -counterpart of fig. 5, shows the consistency between empirical and analytical sensitivity results. Note that the electrode SOC limits always increase with the lithium inventory as implied by figs. 6a and 6c, which is also consistent with fig. 4.

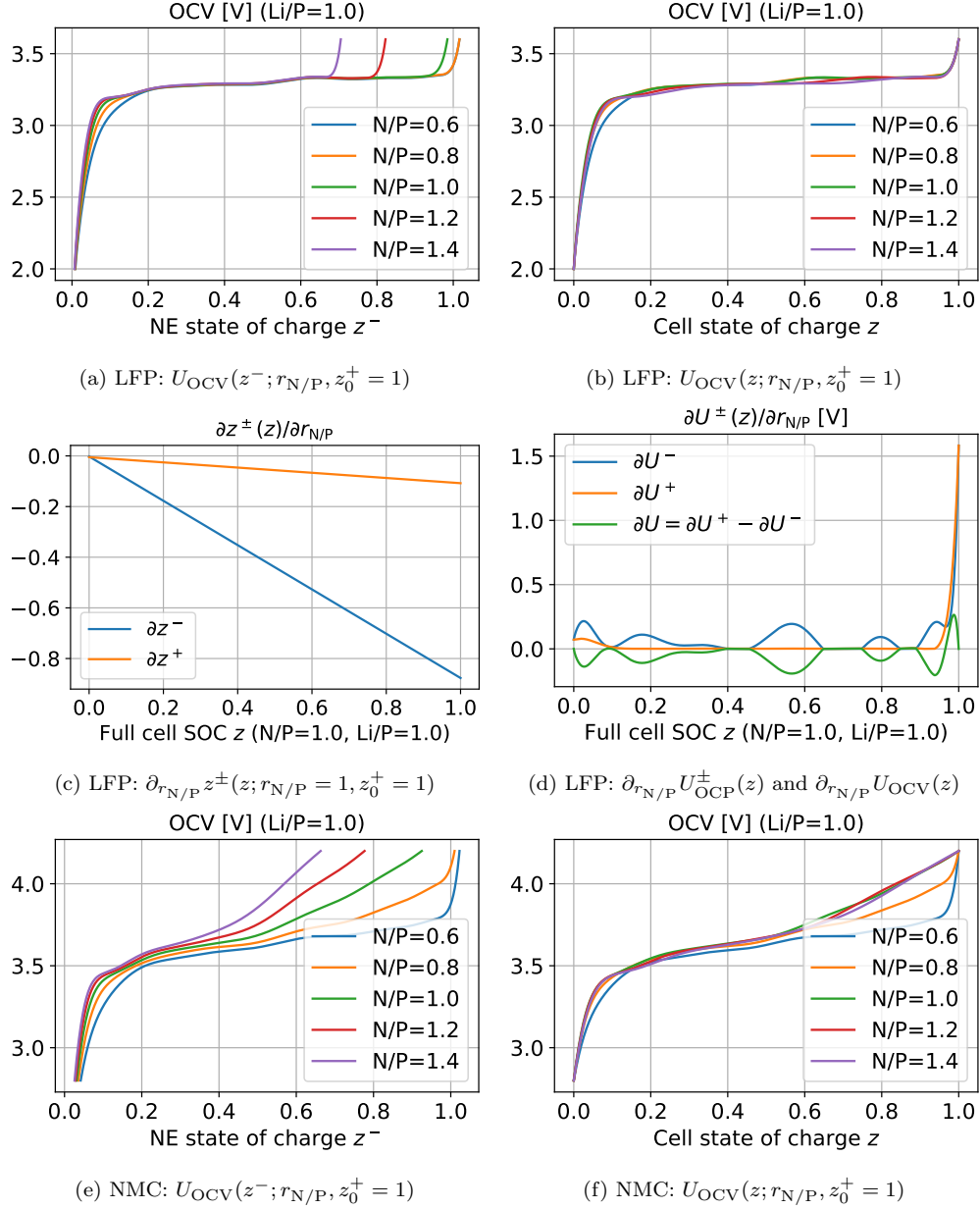


Figure 5: **(a, b)** Variation of NE SOC  $z^-$ -based (left) and cell SOC  $z$ -based (right) cell OCV when  $r_{N/P}$  changes and  $z_0^+ = 1$ . **(c, d)** Derivative-based local sensitivity of  $z^\pm(z)$  (left) and of  $z$ -based electrode OCPs and cell OCV (right) with respect to  $r_{N/P}$ . All the sensitivity derivatives are evaluated at  $r_{N/P} = 1$  and  $z_0^+ = 1$ . **(e, f)** NMC/MCMB counterparts of (a, b).

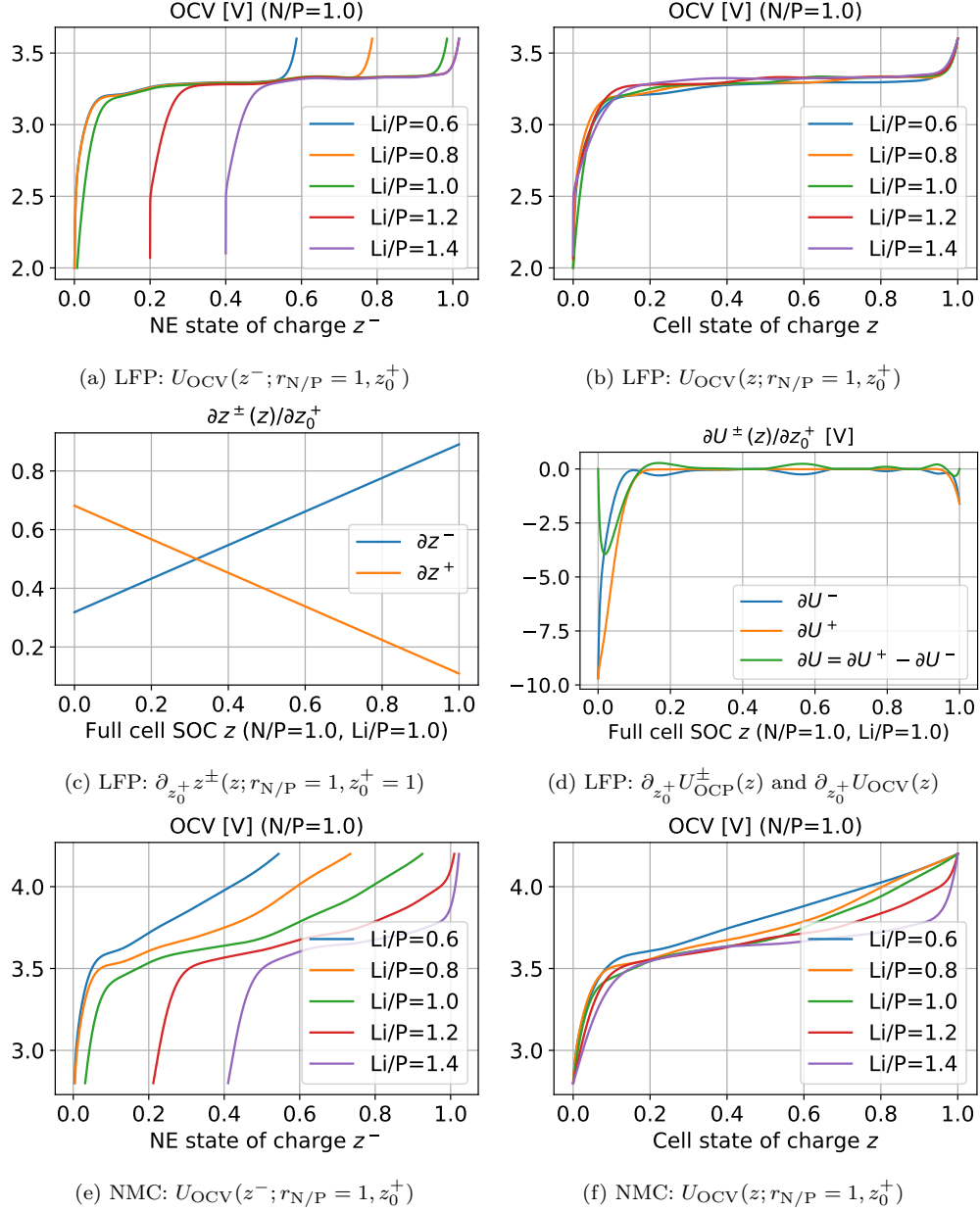


Figure 6: **(a, b)** Variation of NE SOC  $z^-$ -based (left) and cell SOC  $z$ -based (right) cell OCV when Li/P ratio  $z_0^+$  changes and  $r_{N/P} = 1$ . **(c, d)** Derivative-based local sensitivity of  $z^\pm(z)$  (left) and of  $z$ -based electrode OCPs and cell OCV (right) with respect to  $z_0^+$ . All the sensitivity derivatives are evaluated at  $r_{N/P} = 1$  and  $z_0^+ = 1$ . **(e, f)** NMC/MCMB counterparts of (a, b).

### 2.6. Total Capacity without Cutoff Voltage: Four Characteristic Regimes

The cell total capacity  $\hat{Q}_{\max}$  is typically associated with an OCV window, so its sensitivity to SOH parameters such as  $\hat{Q}_{\max}^{\text{Li}}$  and  $\hat{Q}_{\max}^{\pm}$  will inevitably be complicated by the relative contributions of the two electrodes to the OCV slope, as the previous sensitivity gradients are. Before diving into this case, here we will first look into an ideal total capacity  $Q_{\max}$  defined solely by exhausting the usable electrode SOC range, irrespective of the voltage, which will be compared later to the case with a voltage window.

To exhaust the usable SOC range without over-lithiation or over-delithiation, a cell is discharged until either  $z^+$  reaches 1 or  $z^-$  reaches 0, whichever is earlier. Likewise, a cell is charged until one of  $z^+$  reaching 0 and  $z^-$  reaching 1 occurs. By eq. (7), we can work out the criterion determining which alternative is the case as listed in table 3.

Fully discharged			Fully charged		
	$z_{\min}^-$	$z_{\max}^+$	$z_{\max}^-$	$z_{\min}^+$	
Li/P > 1	(Li - P)/N	1	Li/N > 1	1	(Li - N)/P
Li/P ≤ 1	0	Li/P	Li/N ≤ 1	Li/N	0

Table 3: Electrode SOC limits at the ideal case. Note that the Li/P ratio is  $z_0^+$  and the Li/N ratio is  $z_0^+/r_{\text{N/P}}$ . We also use Li, N, and P as shorthand notations for  $\hat{Q}_{\max}^{\text{Li}}$ ,  $\hat{Q}_{\max}^-$ , and  $\hat{Q}_{\max}^+$ , respectively.

The combinations of the two alternatives in each state naturally give rise to four regimes where the ideal total capacity  $Q_{\max} = \hat{Q}_{\max}^-(z_{\max}^- - z_{\min}^-)$  translates to different expressions that depend on  $\hat{Q}_{\max}^{\text{Li}}$  and  $\hat{Q}_{\max}^{\pm}$  differently, as tabulated in table 4.

	Li ≥ N	Li < N
<b>Li ≥ P</b>	Li > N, P $Q_{\max} = N + P - \text{Li}$	N > Li > P $Q_{\max} = P$
<b>Li &lt; P</b>	P > Li > N $Q_{\max} = N$	Li < N, P $Q_{\max} = \text{Li}$

Table 4: Four regimes of dependence of ideal cell total capacity  $Q_{\max}$  on lithium inventory  $\hat{Q}_{\max}^{\text{Li}}$  and active materials  $\hat{Q}_{\max}^{\pm}$ . The four regimes are divided by the relative amount between  $\hat{Q}_{\max}^{\text{Li}}$  and  $\hat{Q}_{\max}^-$  and between  $\hat{Q}_{\max}^{\text{Li}}$  and  $\hat{Q}_{\max}^+$ . The Li/N ratio determines whether the end-of-charge is limited by NE filling up or PE being emptied, and  $\hat{Q}_{\max}^-$  is only identifiable when NE is limiting end-of-charge. Likewise, the Li/P ratio determines whether the end-of-discharge is limited by PE filling up or NE being emptied, and  $\hat{Q}_{\max}^+$  is only identifiable when PE is limiting end-of-discharge. In contrast,  $\hat{Q}_{\max}^{\text{Li}}$  is only identifiable when the two ratio are both larger or smaller than 1, where the surplus and lack of lithium become the capacity bottleneck, respectively.

Dubarry and Anseán [20] discuss in their figure 6 the relative capacity loss expressions when the start and end state fall into each of these four regimes. Here we further elucidate the criteria that determine which regime a cell is in and derive a simple expression directly relating the total capacity to the SOH parameters. Our results also reveal the counter-intuitive negative dependence of total capacity on lithium inventory when there is a surplus of the latter, which is missed in previous work and will be discussed in more detail later.

### 2.7. SOH-Sensitivity Gradients of Cutoff-Voltage-Based Total Capacity: Four Characteristic Regimes

Besides for the cell OCV  $U_{\text{OCV}}(z)$ , we can also compute the sensitivity derivatives for the total capacity  $\hat{Q}_{\max} = (z_{\max}^- - z_{\min}^-)r_{\text{N/P}}\hat{Q}_{\max}^+$  by eq. (23). Note, however, that besides the dimensionless

$r_{\text{N/P}}$  and  $z_0^+$ ,  $\hat{Q}_{\text{max}}$  also depends on the dimensional  $\hat{Q}_{\text{max}}^+$ . Therefore, for  $\hat{Q}_{\text{max}}(r_{\text{N/P}}, z_0^+, \hat{Q}_{\text{max}}^+)$ , we can obtain the following parameter-derivatives:

$$\frac{\partial \hat{Q}_{\text{max}}}{\partial r_{\text{N/P}}} = (z_{\text{max}}^- \lambda_{\text{u}}^- - z_{\text{min}}^- \lambda_{\text{l}}^-) \hat{Q}_{\text{max}}^+, \quad \frac{\partial \hat{Q}_{\text{max}}}{\partial z_0^+} = (\lambda_{\text{u}}^+ - \lambda_{\text{l}}^+) \hat{Q}_{\text{max}}^+, \quad \frac{\partial \hat{Q}_{\text{max}}}{\partial \hat{Q}_{\text{max}}^+} = (z_{\text{max}}^- - z_{\text{min}}^-) r_{\text{N/P}} \quad (41)$$

where we have used eqs. (34) and (38).

In contrast to  $U_{\text{OCV}}(z)$ , the total capacity  $\hat{Q}_{\text{max}}$  can be alternatively parametrized by  $\hat{Q}_{\text{max}}^{\text{Li}}$ ,  $\hat{Q}_{\text{max}}^-$ , and  $\hat{Q}_{\text{max}}^+$ , all of which are of the same dimension of charges. To derive the parametric derivatives for this case, one subtlety is that we need to translate  $z^+(z^-; r_{\text{N/P}}, z_0^+)$  to

$$z^+(z^-; \hat{Q}_{\text{max}}^{\text{Li}}, \hat{Q}_{\text{max}}^-, \hat{Q}_{\text{max}}^+) = \frac{\hat{Q}_{\text{max}}^{\text{Li}}}{\hat{Q}_{\text{max}}^+} - \frac{\hat{Q}_{\text{max}}^-}{\hat{Q}_{\text{max}}^+} z^-, \quad (42)$$

which yields

$$\frac{\partial z^+(z^-)}{\partial \hat{Q}_{\text{max}}^{\text{Li}}} = \frac{1}{\hat{Q}_{\text{max}}^+}, \quad \frac{\partial z^+(z^-)}{\partial \hat{Q}_{\text{max}}^-} = \frac{-z^-}{\hat{Q}_{\text{max}}^+}, \quad \frac{\partial z^+(z^-)}{\partial \hat{Q}_{\text{max}}^+} = \frac{-z^+}{\hat{Q}_{\text{max}}^+}. \quad (43)$$

Note that in deriving (41), we have implicitly used

$$\frac{\partial z^+(z^-; r_{\text{N/P}}, z_0^+, \hat{Q}_{\text{max}}^+)}{\partial \hat{Q}_{\text{max}}^+} = 0 \neq \frac{\partial z^+(z^-; \hat{Q}_{\text{max}}^{\text{Li}}, \hat{Q}_{\text{max}}^-, \hat{Q}_{\text{max}}^+)}{\partial \hat{Q}_{\text{max}}^+},$$

which exemplifies the partial differentiation ambiguity without specifying the complete parametrization as mentioned. Now using eq. (31), we have

$$\frac{\partial z_{\text{min}}^-}{\partial \hat{Q}_{\text{max}}^{\text{Li}}} = \frac{\lambda_{\text{l}}^+}{\hat{Q}_{\text{max}}^-}, \quad \frac{\partial z_{\text{max}}^-}{\partial \hat{Q}_{\text{max}}^{\text{Li}}} = \frac{\lambda_{\text{u}}^+}{\hat{Q}_{\text{max}}^-}, \quad (44)$$

$$\frac{\partial z_{\text{min}}^-}{\partial \hat{Q}_{\text{max}}^-} = \frac{-z_{\text{min}}^- \lambda_{\text{l}}^+}{\hat{Q}_{\text{max}}^-}, \quad \frac{\partial z_{\text{max}}^-}{\partial \hat{Q}_{\text{max}}^-} = \frac{-z_{\text{max}}^- \lambda_{\text{u}}^+}{\hat{Q}_{\text{max}}^-}, \quad (45)$$

$$\frac{\partial z_{\text{min}}^-}{\partial \hat{Q}_{\text{max}}^+} = \frac{-z_{\text{max}}^+ \lambda_{\text{l}}^+}{\hat{Q}_{\text{max}}^-}, \quad \frac{\partial z_{\text{max}}^-}{\partial \hat{Q}_{\text{max}}^+} = \frac{-z_{\text{min}}^+ \lambda_{\text{u}}^+}{\hat{Q}_{\text{max}}^-}, \quad (46)$$

which by eq. (23), finally give the sensitivity derivatives:

$$\frac{\partial \hat{Q}_{\text{max}}}{\partial \hat{Q}_{\text{max}}^{\text{Li}}} = \lambda_{\text{u}}^+ - \lambda_{\text{l}}^+, \quad \frac{\partial \hat{Q}_{\text{max}}}{\partial \hat{Q}_{\text{max}}^-} = z_{\text{max}}^- \lambda_{\text{u}}^- - z_{\text{min}}^- \lambda_{\text{l}}^-, \quad \frac{\partial \hat{Q}_{\text{max}}}{\partial \hat{Q}_{\text{max}}^+} = z_{\text{max}}^+ \lambda_{\text{l}}^+ - z_{\text{min}}^+ \lambda_{\text{u}}^+. \quad (47)$$

There are several advantages of the above all-capacity parametrization. First, it is conceptually straightforward because the cell total capacity  $\hat{Q}_{\text{max}}$  is the direct result of the synergy between the lithium inventory  $\hat{Q}_{\text{max}}^{\text{Li}}$ , the anode capacity  $\hat{Q}_{\text{max}}^-$ , and the cathode capacity  $\hat{Q}_{\text{max}}^+$ . Moreover, all of them are of the same dimension and thus directly comparable, which also makes the parametric derivatives dimensionless and intuitive with values being readily interpretable. For example,  $\frac{\partial \hat{Q}_{\text{max}}}{\partial \hat{Q}_{\text{max}}^-}$  indicates the fraction of NE capacity change that indeed manifests in cell total capacity. As a result, the three derivatives in eq. (47) can be used to indicate to what extent each factor is the bottleneck dominating the change of total capacity. A derivative  $\frac{\partial \hat{Q}_{\text{max}}}{\partial Q}$  close to 1 implies the factor being limiting, while a value close to 0 hints the opposite.

Interestingly, if we examine the sign and range of these three derivatives carefully, we can find that they are not necessarily positive. We know that  $0 \leq \lambda^+ \leq 1$ , and if each electrode potential window covers the whole active range in operation as is typically the case, we also have  $0 \leq z_{\min}^\pm < z_{\max}^\pm \leq 1$ . Under these conditions, we have the following bounds:

$$-1 \leq \partial_{\hat{Q}_{\max}^{\text{Li}}} \hat{Q}_{\max}, \partial_{\hat{Q}_{\max}^-} \hat{Q}_{\max}, \partial_{\hat{Q}_{\max}^+} \hat{Q}_{\max} \leq 1. \quad (48)$$

Moreover,  $z_{\min}^\pm$  is often close to 0 while  $z_{\max}^\pm$  close to 1, so typically we should have

$$\partial_{\hat{Q}_{\max}^-} \hat{Q}_{\max}, \partial_{\hat{Q}_{\max}^+} \hat{Q}_{\max} \geq 0,$$

and they will hardly be much smaller than 0 even if they ever become negative. A negative derivative of this kind simply means loss of active materials or lithium inventory will, counterintuitively, increase the total capacity.

For lithium inventory  $\hat{Q}_{\max}^{\text{Li}}$ , it is actually not hard to imagine such a case. Cell total capacity indicates the amount of  $\text{Li}^+$  that can be shuttled from one electrode to the other, so too few  $\text{Li}^+$  will definitely limit the capacity, but so will too many  $\text{Li}^+$  because there will be no space for them to move, so both electrodes easily get filled up. In that case, discharging is PE-limited so  $\lambda_1^+ \approx 1$ , while charging is NE-limited so  $\lambda_u^+ \approx 0$ , and the two together yield  $\partial_{\hat{Q}_{\max}^{\text{Li}}} \hat{Q}_{\max} \approx -1$ . It is therefore intuitive why loss of lithium inventory in such scenarios will boost the total capacity. However, it should also be noted that a normal cell rarely falls into this regime because in typical cell assembly, only the PE is filled with  $\text{Li}^+$  while the NE is totally  $\text{Li}^+$ -free. A cell with surplus lithium is usually manufactured deliberately by prelithiating the NE before the assembly [3].

Note that although  $\hat{Q}_{\max}$  depends on all three of  $\hat{Q}_{\max}^{\text{Li}}$ ,  $\hat{Q}_{\max}^-$ , and  $\hat{Q}_{\max}^+$ , the dimensionless derivatives in (47) only depend on the also dimensionless  $r_{\text{N/P}}$  and  $z_0^+$ . Therefore, we can visualize the different regimes of a cell where the total capacity is limited by the three components to different extents by plotting the three profiles of  $\partial_{\hat{Q}_{\max}^{(\cdot)}} \hat{Q}_{\max}(r_{\text{N/P}}, z_0^+)$  as shown in fig. 7. If we look at figs. 4 and 7 together, we can see how the four-quadrant pattern from  $z_{\min/\max}^\pm$  and  $\lambda_{l/u}^+$  propagates into  $\partial_{\hat{Q}_{\max}^{(\cdot)}} \hat{Q}_{\max}$  through (47).

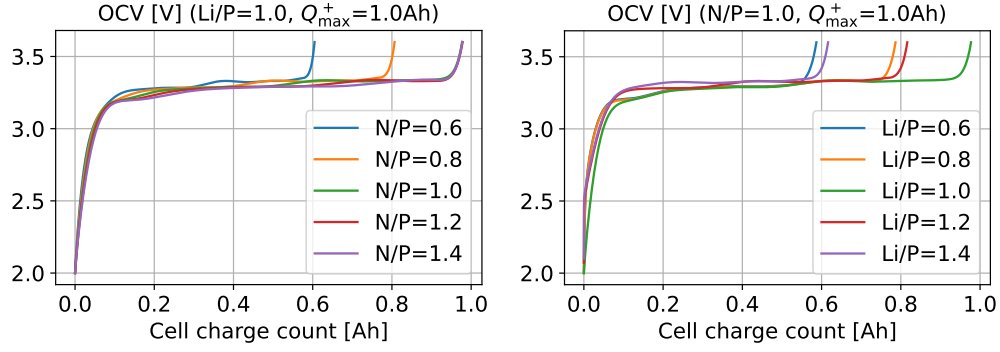
The characteristics of the four SOH regimes are summarized in table 5. In conclusion, the four regimes are divided by the relative amount between  $\hat{Q}_{\max}^{\text{Li}}$  and  $\hat{Q}_{\max}^-$  and between  $\hat{Q}_{\max}^{\text{Li}}$  and  $\hat{Q}_{\max}^+$ . The Li/N ratio determines whether the end-of-charge is limited by NE filling up or PE being emptied, and  $\hat{Q}_{\max}^-$  is highly identifiable when NE is limiting end-of-charge. Likewise, the Li/P ratio determines whether the end-of-discharge is limited by PE filling up or NE being emptied, and  $\hat{Q}_{\max}^+$  is highly identifiable when PE is limiting end-of-discharge. In contrast,  $\hat{Q}_{\max}^{\text{Li}}$  is highly identifiable when the two ratio are both larger or smaller than 1, where the surplus and lack of lithium become the capacity bottleneck, respectively.

On the other hand, the other parametrization  $\hat{Q}_{\max}(r_{\text{N/P}}, z_0^+, \hat{Q}_{\max}^+)$  is not without advantage. We know the  $z$ -based cell OCV  $U_{\text{OCV}}(z)$  depends on  $r_{\text{N/P}}$  and  $z_0^+$  only, and  $\hat{Q}_{\max}^+$  only comes into the picture when the cell total capacity  $\hat{Q}_{\max}$  is concerned. Therefore, the original parametrization confines all the dimensional contributions to  $\hat{Q}_{\max}$  within the single  $\hat{Q}_{\max}^+$ , which is structurally more aligned with the underlying parametric dependence.

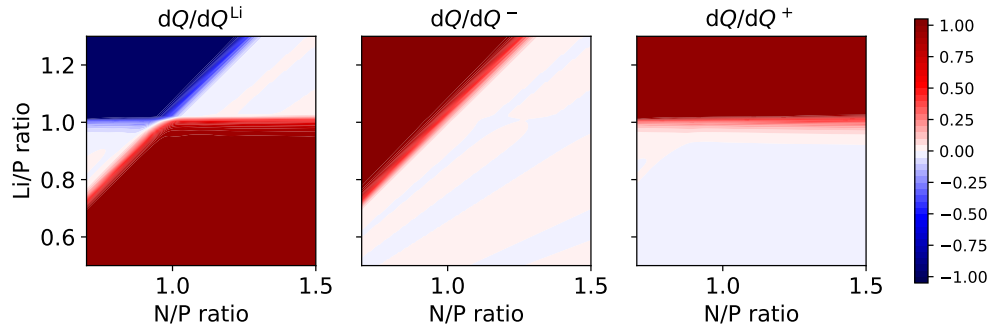
### 3. Applications of Analytic Sensitivity

To quantify identifiability is essentially to revert the parameter-to-measurement forward sensitivity, and there are different approaches to this inversion. A straightforward approach is to

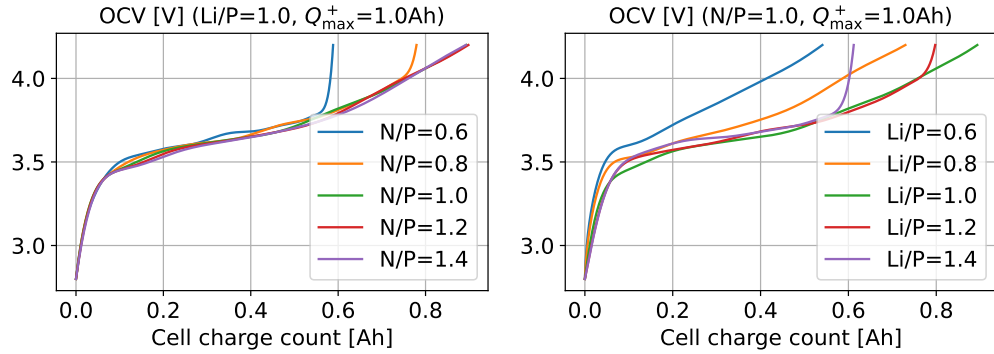




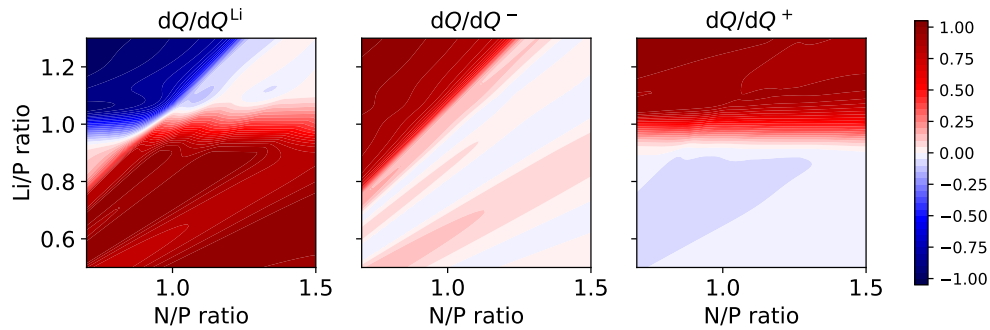
(a) LFP:  $U_{OCV}(Q_c; r_{N/P}, z_0^+ = 1, \hat{Q}_{\max}^+ = 1\text{Ah})$  (b) LFP:  $U_{OCV}(Q_c; r_{N/P} = 1, z_0^+, \hat{Q}_{\max}^+ = 1\text{Ah})$



(c) LFP:  $\partial_{\hat{Q}_{\max}^{\text{Li}}} \hat{Q}_{\max}$ ,  $\partial_{\hat{Q}_{\max}^-} \hat{Q}_{\max}$ , and  $\partial_{\hat{Q}_{\max}^+} \hat{Q}_{\max}$



(d) NMC:  $U_{OCV}(Q_c; r_{N/P}, z_0^+ = 1, \hat{Q}_{\max}^+ = 1\text{Ah})$  (e) NMC:  $U_{OCV}(Q_c; r_{N/P} = 1, z_0^+, \hat{Q}_{\max}^+ = 1\text{Ah})$



(f) NMC:  $\partial_{\hat{Q}_{\max}^{\text{Li}}} \hat{Q}_{\max}$ ,  $\partial_{\hat{Q}_{\max}^-} \hat{Q}_{\max}$ , and  $\partial_{\hat{Q}_{\max}^+} \hat{Q}_{\max}$

Figure 7: (a, b) Variation of  $Q_c$ -based cell OCV and total capacity  $\hat{Q}_{\max}$  when  $r_{N/P}$  changes and  $z_0^+ = 1$  (left) and when  $z_0^+$  changes and  $r_{N/P} = 1$  (right), both assuming  $\hat{Q}_{\max}^+ = 1\text{Ah}$ . For the former case, this implies that  $\hat{Q}_{\max}^-$  changes while  $\hat{Q}_{\max}^{\text{Li}} = \hat{Q}_{\max}^+ = 1\text{Ah}$ . (c) Gradient-based sensitivity of total capacity with respect to the amount of lithium inventory, NE, and PE active materials at different  $(r_{N/P}, z_0^+)$  pairs. (d, e, f) NMC/MCMB counterparts of (a, b, c).

		<b>Li &gt; N</b>	<b>Li &lt; N</b>
		$\lambda_u^- \rightarrow 1, \quad \partial_{\hat{Q}_{\max}^-} \hat{Q}_{\max} \rightarrow 1$	$\lambda_u^- \rightarrow 0, \quad \partial_{\hat{Q}_{\max}^-} \hat{Q}_{\max} \rightarrow 0$
<b>Li &gt; P</b>	$\lambda_l^+ \rightarrow 1, \quad \partial_{\hat{Q}_{\max}^+} \hat{Q}_{\max} \rightarrow 1$	$\hat{Q}_{\max}^{\text{Li}} > \hat{Q}_{\max}^{\pm}$ $\partial_{\hat{Q}_{\max}^{\text{Li}}} \hat{Q}_{\max} \rightarrow -1$	$\hat{Q}_{\max}^- > \hat{Q}_{\max}^{\text{Li}} > \hat{Q}_{\max}^+$ $\partial_{\hat{Q}_{\max}^{\text{Li}}} \hat{Q}_{\max} \rightarrow 0$
<b>Li &lt; P</b>	$\lambda_l^+ \rightarrow 0, \quad \partial_{\hat{Q}_{\max}^+} \hat{Q}_{\max} \rightarrow 0$	$\hat{Q}_{\max}^+ > \hat{Q}_{\max}^{\text{Li}} > \hat{Q}_{\max}^-$ $\partial_{\hat{Q}_{\max}^{\text{Li}}} \hat{Q}_{\max} \rightarrow 0$	$\hat{Q}_{\max}^{\text{Li}} < \hat{Q}_{\max}^{\pm}$ $\partial_{\hat{Q}_{\max}^{\text{Li}}} \hat{Q}_{\max} \rightarrow 1$

Table 5: Four regimes of sensitivity of cell total capacity  $\hat{Q}_{\max}$  to lithium inventory  $\hat{Q}_{\max}^{\text{Li}}$  and active materials  $\hat{Q}_{\max}^{\pm}$ . Compare to table 4.

devise an estimator and calibrate the estimation error by feeding measurements coming from a known ground truth [3, 19]. The drawback of this approach is that it entangles the identifiability intrinsic to the problem with the error incurred by the estimator itself. If real data are used, the imperfectness of the model used will further complicate the apparent identifiability.

To study only the identifiability intrinsic to a problem, one simple approach is based on the sensitivity gradients, as we shall adopt here. However, this approach only concerns how the measurements vary with the parameters locally. To quantify global identifiability, more sophisticated techniques such as those based on Bayesian inversion are needed [26].

### 3.1. N/P and Li/P Identifiability from SOC-Based OCV Measurements by Fisher Information

One immediate application of the sensitivity gradients is to quantify the minimal estimation errors in the latent SOH parameters from noisy voltage measurements. The simple idea is if we measure  $y = f(\theta)$  with standard error  $\sigma_y$  to estimate  $\theta$ , and we know  $\theta$  and  $y$  are close to some  $\theta_0$  and  $y_0 = f(\theta_0)$ , respectively, we can linearize  $f(\theta)$  around  $\theta_0$  and thus  $\sigma_y/\sigma_\theta = d_\theta f(\theta_0)$ , which yields a standard error  $\sigma_\theta = \sigma_y/d_\theta f(\theta_0)$ . When this is generalized to the vector case with  $m$  measurements  $\mathbf{y} = \mathbf{f}(\boldsymbol{\theta}) \in \mathbb{R}^m$  and  $d$  underlying parameters  $\boldsymbol{\theta} \in \mathbb{R}^d$ , the derivative becomes the Jacobi matrix  $\nabla_{\boldsymbol{\theta}} \mathbf{f} \in \mathbb{R}^{m \times d}$  and the  $\sigma_y^2$  and  $\sigma_\theta^2$  become the error covariance  $\mathbf{C}_y \in \mathbb{R}^{m \times m}$  and  $\mathbf{C}_\theta \in \mathbb{R}^{d \times d}$ , respectively. Aided by a square root of the symmetric positive definite  $\mathbf{C}_y$ , we can obtain the vector counterpart of  $\sigma_\theta = \sigma_y/d_\theta f(\theta_0)$  as

$$\mathbf{C}_\theta^{-1}(\boldsymbol{\theta}_0) = \nabla_{\boldsymbol{\theta}}^T \mathbf{f}(\boldsymbol{\theta}_0) \mathbf{C}_y^{-1} \nabla_{\boldsymbol{\theta}} \mathbf{f}(\boldsymbol{\theta}_0). \quad (49)$$

If we solve the weighted NLS (nonlinear least squares) to obtain

$$\boldsymbol{\theta}_*(\hat{\mathbf{y}}) = \arg \min_{\boldsymbol{\theta}} (\mathbf{f}(\boldsymbol{\theta}) - \hat{\mathbf{y}})^T \mathbf{C}_y^{-1} (\mathbf{f}(\boldsymbol{\theta}) - \hat{\mathbf{y}}), \quad (50)$$

where  $\hat{\mathbf{y}}$  are actual measured values of  $\mathbf{y}$ , substituting  $\boldsymbol{\theta}_*$  to  $\boldsymbol{\theta}_0$  in (49) yields a standard error covariance for the optimizer  $\boldsymbol{\theta}_*$ . Note, however, that such gradient-based identifiability results are only valid locally and are based on the premise that  $\boldsymbol{\theta}_*$  is near the ground truth  $\boldsymbol{\theta}_{\text{tr}}$  and  $\hat{\mathbf{y}}$  are noisy unbiased measurements of  $\mathbf{f}(\boldsymbol{\theta}_{\text{tr}})$  with covariance  $\mathbf{C}_y$ . If the nonlinear optimization does not ever get close to  $\boldsymbol{\theta}_{\text{tr}}$ , of course the above results are irrelevant to how close  $\boldsymbol{\theta}_*$  is to  $\boldsymbol{\theta}_{\text{tr}}$ .

When the weighted NLS optimizer  $\boldsymbol{\theta}_*$  is equivalently formulated as the maximum likelihood estimator  $\boldsymbol{\theta}_*(\hat{\mathbf{y}}) = \arg \max_{\boldsymbol{\theta}} p(\hat{\mathbf{y}}|\boldsymbol{\theta})$  with a Gaussian likelihood  $\mathbf{y}|\boldsymbol{\theta} \sim \mathcal{N}(\mathbf{f}(\boldsymbol{\theta}), \mathbf{C}_y)$ , (49) turns out to be the well known Fisher information matrix [27]

$$\mathbf{F}_y(\boldsymbol{\theta}_*) = \mathbb{E}_{\mathbf{y}|\boldsymbol{\theta}_*} [\nabla_{\boldsymbol{\theta}}^T \ln p(\mathbf{y}|\boldsymbol{\theta}_*) \nabla_{\boldsymbol{\theta}} \ln p(\mathbf{y}|\boldsymbol{\theta}_*)] = \nabla_{\boldsymbol{\theta}}^T \mathbf{f}(\boldsymbol{\theta}_*) \mathbf{C}_y^{-1} \nabla_{\boldsymbol{\theta}} \mathbf{f}(\boldsymbol{\theta}_*). \quad (51)$$

Under this probabilistic framework, the inverse Fisher information matrix is the Cramér-Rao lower bound of the covariance of all unbiased estimator  $\hat{\boldsymbol{\theta}}(\hat{y})$ , i.e.  $(\text{Cov}(\hat{\boldsymbol{\theta}}(\hat{y})) - \mathbf{F}_y^{-1}(\boldsymbol{\theta}_{\text{tr}}))$  is semi-positive definite [28, sec. 11.10]. Although we do not know  $\boldsymbol{\theta}_{\text{tr}}$  in practice, and the maximum likelihood estimator  $\boldsymbol{\theta}_*(\hat{y})$  is not necessarily unbiased, we can still use the inverse of (51) as a semi-heuristic error covariance, as [11, 15] have done for their OCV model parametrization (4). Due to the cutoff-voltage constraint between the two electrode SOC limits in their parameters, extra treatments are needed to evaluate the Fisher information matrix. The independent and cutoff-voltage-agnostic parametrization introduced in this work allows this to be done with more ease.

In practice, we can usually assume that the errors in different measurements are independent, which translates to  $\mathbf{C}_y = \text{Diag}(\sigma_{y_i}^2)$  being diagonal. In this case, the contributions of different measurements to  $\mathbf{C}_\theta^{-1}$  become additive rank-1 updates:

$$\mathbf{C}_\theta^{-1} = \sum_{i=1}^m \frac{1}{\sigma_{y_i}^2} \nabla_{\boldsymbol{\theta}}^T f_i(\boldsymbol{\theta}_0) \nabla_{\boldsymbol{\theta}} f_i(\boldsymbol{\theta}_0). \quad (52)$$

If a complete OCV curve has been observed, naturally the total capacity  $\hat{Q}_{\text{max}}$  is also directly measured by Coulomb counting. What remains to be done is identifying the N/P and Li/P ratio  $\boldsymbol{\theta} = [r_{\text{N/P}}, z_0^+]$  from the  $(z_i, \hat{U}_i)$  pairs. Assume  $z_i$  is accurate and every  $\hat{U}_i$  has a standard error  $\sigma_U$ . Since  $f_i(\boldsymbol{\theta}) = U_{\text{OCV}}(z_i; r_{\text{N/P}}, z_0^+)$  here, we have

$$\nabla_{\boldsymbol{\theta}} U_{\text{OCV}}(z_i) = [\partial_{r_{\text{N/P}}} U_{\text{OCV}}(z_i), \partial_{z_0^+} U_{\text{OCV}}(z_i)], \quad (53)$$

which together with (52) evaluated at the NLS optimizer  $\boldsymbol{\theta}_*$  yields error covariance for  $[r_{\text{N/P}}, z_0^+]$ .

The above results are applied to the same LFP-graphite chemistry as used before with four different  $(r_{\text{N/P}}, z_0^+)$  pairs to examine how informative OCV measurements from certain SOC windows are about the N/P ratio  $r_{\text{N/P}}$  and Li/P ratio  $z_0^+$ , as shown in fig. 8. We choose the OCV at SOC  $z = 1\%, 2\%, \dots, 99\%$  as candidate measurements and traverse every SOC window  $[z_{\text{lower}}, z_{\text{upper}}]$  with ends from them that contains at least two measurements. The standard error of OCV measurements is assumed to be  $\sigma_U = 5\text{mV}$ , and the standard estimation errors of  $r_{\text{N/P}}$  and  $z_0^+$  for each SOC window obtained by the square root of  $\text{diag}(\mathbf{C}_\theta)$  are demonstrated in each sub-figure of fig. 8. We limit the color bar to the range of  $[0.0, 0.2]$  to visualize the practically relevant features, because a standard error larger than 0.2 for  $r_{\text{N/P}}$  and  $z_0^+$  having a value around 1 means the estimation is almost useless. On the other hand, the OCV model is not perfect in practice, and model errors will limit the estimation accuracy in the first place, so we consider an estimation error of under 0.01 in this ideal setup as more than enough. Hence, in fig. 8, a dark zone indicates small-enough errors while a bright zone implies ineffective estimation.

Note that if one SOC window is nested in another, the OCV measurements of the latter also contain all those in the former, so the estimation error is monotonically decreasing vertically and increasing horizontally. Moreover, we see the errors having a sharp change in certain SOC, indicating the OCV measurements at such SOC to be particularly sensitive to  $r_{\text{N/P}}$  and  $z_0^+$ , agreeing with figs. 5d and 6d. We can also observe that estimating  $r_{\text{N/P}}$  is harder than estimating  $z_0^+$  in most cases here, which is consistent with figs. 2b and 2d, and OCV values at lower SOC are overall more informative than those at high SOC. Finally, it is also obvious that the SOH parameter identifiability is significantly higher for NMC than for LFP, aligned with the larger empirical sensitivity to SOH parameter perturbation we have visualized previously.

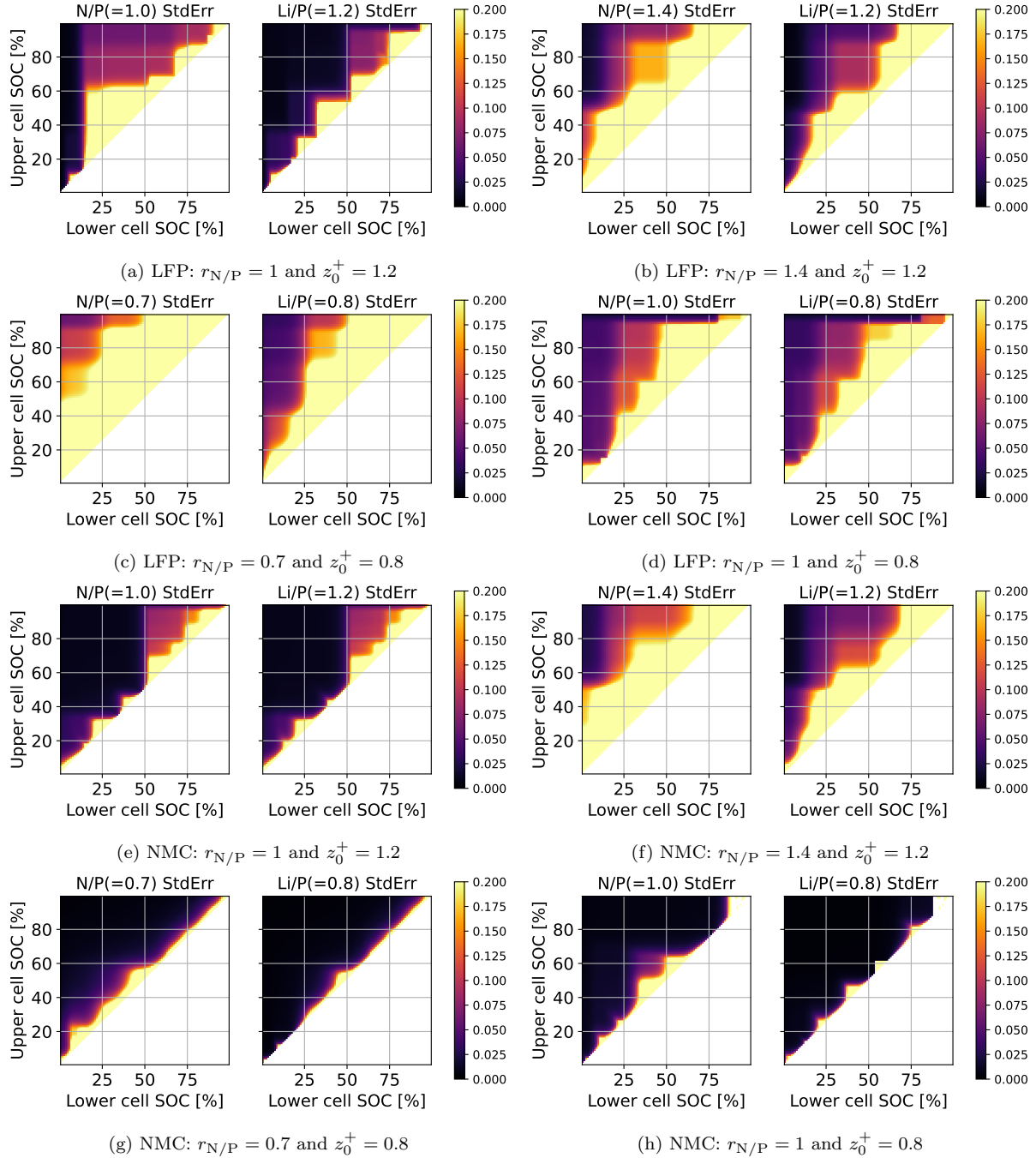


Figure 8: Standard estimation errors of the N/P ratio  $r_{N/P}$  and Li/P ratio  $z_0^+$  based on OCV measurements sampled at every 1% SOC within any cell SOC window  $[z_{lower}, z_{upper}]$  at least 1% apart. The errors are obtained as the square root of the diagonals of the inverse Fisher information matrix evaluated at different pairs of  $(r_{N/P}, z_0^+)$  values corresponding to the four regimes discussed in section 2.7. The standard OCV measurement error is assumed to be  $\sigma_U = 5\text{mV}$ . (a, b, c, d) LFP/MCMB results. (e, f, g, h) NMC/MCMB counterparts.

### 3.2. Lithium Inventory and Active Material Identifiability from Charge-Based OCV Measurements by Fisher Information

The previous case of measuring the SOC-based  $U_{\text{OCV}}(z)$  requires the whole OCV curve, which may not be available in some scenarios. Given only partial OCV curve measurements, we must work with the raw data of OCV versus charge throughput, say  $Q_c$  counted from some initial state at  $U_{\text{OCV}} = U_{\text{ini}}$  and is positive in the charging direction, because relating  $Q_c$  to the full cell SOC  $z$  requires knowing the SOH parameters of the lithium inventory  $\hat{Q}_{\text{max}}^{\text{Li}}$  and the NE and PE active material amount  $\hat{Q}_{\text{max}}^{\pm}$ , or their equivalent re-parametrization, which are being sought after in the first place.

Suppose  $Q_c = 0$  corresponds to some known initial voltage  $U_{\text{OCV}} = U_{\text{ini}}$ . The charge-based OCV relation becomes

$$U_{\text{OCV}}(Q_c) = U_{\text{OCP}}^+(z_{\text{ini}}^+(z_{\text{ini}}^-(U_{\text{ini}})) - Q_c/\hat{Q}_{\text{max}}^+) - U_{\text{OCP}}^-(z_{\text{ini}}^-(U_{\text{ini}}) + Q_c/\hat{Q}_{\text{max}}^-), \quad (54)$$

where the  $z_{\text{ini}}^+(z_{\text{ini}}^-)$  dependence comes from eq. (7) while the  $z_{\text{ini}}^-(U_{\text{ini}})$  dependence is inverted from eq. (9), both of which parametrized by the N/P ratio  $r_{\text{N/P}}$  and Li/P ratio  $z_0^+$ .

Note that if a quantity  $f$  is parametrized by  $r_{\text{N/P}}$  and  $z_0^+$ , since

$$f(r_{\text{N/P}}, z_0^+) = f(\hat{Q}_{\text{max}}^-/\hat{Q}_{\text{max}}^+, \hat{Q}_{\text{max}}^{\text{Li}}/\hat{Q}_{\text{max}}^+),$$

$f$  can also be viewed as being, though less parsimoniously, parametrized by  $\hat{Q}_{\text{max}}^{\text{Li}}$  and  $\hat{Q}_{\text{max}}^{\pm}$ . Hence,

$$\frac{\partial f}{\partial \hat{Q}_{\text{max}}^{\text{Li}}} = \frac{1}{\hat{Q}_{\text{max}}^+} \frac{\partial f}{\partial z_0^+}, \quad \frac{\partial f}{\partial \hat{Q}_{\text{max}}^-} = \frac{1}{\hat{Q}_{\text{max}}^+} \frac{\partial f}{\partial r_{\text{N/P}}}, \quad \frac{\partial f}{\partial \hat{Q}_{\text{max}}^{\text{Li}}} = -\frac{\hat{Q}_{\text{max}}^-}{(\hat{Q}_{\text{max}}^+)^2} \frac{\partial f}{\partial r_{\text{N/P}}} - \frac{\hat{Q}_{\text{max}}^{\text{Li}}}{(\hat{Q}_{\text{max}}^+)^2} \frac{\partial f}{\partial z_0^+}. \quad (55)$$

With the aids of the above relations, we can obtain the sensitivity gradient of  $U_{\text{OCV}}(Q_c)$  with respect to  $\hat{Q}_{\text{max}}^{\text{Li}}$  and  $\hat{Q}_{\text{max}}^{\pm}$ :

$$\frac{\partial U_{\text{OCV}}(Q_c)}{\partial \hat{Q}_{\text{max}}^{\text{Li}}} = \frac{\lambda_{\text{ini}}^-}{\hat{Q}_{\text{max}}^+} \frac{dU_{\text{OCP}}^+}{dz^+} - \frac{\lambda_{\text{ini}}^+}{\hat{Q}_{\text{max}}^-} \frac{dU_{\text{OCP}}^-}{dz^-}, \quad (56)$$

$$\frac{\partial U_{\text{OCV}}(Q_c)}{\partial \hat{Q}_{\text{max}}^-} = -\frac{z_{\text{ini}}^- \lambda_{\text{ini}}^-}{\hat{Q}_{\text{max}}^+} \frac{dU_{\text{OCP}}^+}{dz^+} + \frac{z_{\text{ini}}^- \lambda_{\text{ini}}^+ + Q_c/\hat{Q}_{\text{max}}^-}{\hat{Q}_{\text{max}}^-} \frac{dU_{\text{OCP}}^-}{dz^-}, \quad (57)$$

$$\frac{\partial U_{\text{OCV}}(Q_c)}{\partial \hat{Q}_{\text{max}}^+} = \frac{-z_{\text{ini}}^+ \lambda_{\text{ini}}^- + Q_c/\hat{Q}_{\text{max}}^+}{\hat{Q}_{\text{max}}^+} \frac{dU_{\text{OCP}}^+}{dz^+} + \frac{z_{\text{ini}}^+ \lambda_{\text{ini}}^+}{\hat{Q}_{\text{max}}^-} \frac{dU_{\text{OCP}}^-}{dz^-}. \quad (58)$$

With the sensitivity gradient calculated, we can now use the same approach of Fisher information matrix to study the identifiability of  $\hat{Q}_{\text{max}}^{\text{Li}}$  and  $\hat{Q}_{\text{max}}^{\pm}$  from partial OCV measurements from a certain SOC window. For testing purpose, we choose the charge throughput increment  $\Delta Q_c$  to be 1% of the ground truth of the cell total capacity so  $\Delta Q_c$  translates to 1% cell SOC change. Moreover, we choose the starting voltage  $U_{\text{ini}}$  to be the ground truth of cell OCV at each integer cell SOC percentage. This way, each partial segment of OCV measurements can be normalized into an SOC window as in the previous case for more intuitive visualization.

The standard estimation errors are shown in fig. 9 using the same layout as in fig. 8. The overall patterns are similar to those in fig. 8, except that the estimation errors are, though still monotonely increasing along the upper SOC axis, no longer strictly monotonely decreasing along the lower SOC axis, as indicated by the pattern of some vertical downward pointing ‘‘fingers’’. This is because the voltage measurement at a particular cell SOC  $z$  is interpreted differently when the

initial voltage changes, so it is not really the same measurement under such different scenarios. For example, if the starting OCV is  $U_{\text{ini}} = U_{\text{OCV}}(z = 20\%)$ , an OCV measurement at  $z = 60\%$  is interpreted as the OCV reached when the cell is charged from  $U_{\text{OCV}} = U_{\text{ini}}$  by a charge throughput of  $(60\% - 20\%) \hat{Q}_{\text{max}} = 40\% \hat{Q}_{\text{max}}$ . Obviously, such meaning will change along the starting OCV, so the information born by such measurements regarding the underlying SOH parameters are not identical. Such quantities of voltage change across certain charge throughput have also been extracted as features to estimate cell total capacity in literature.

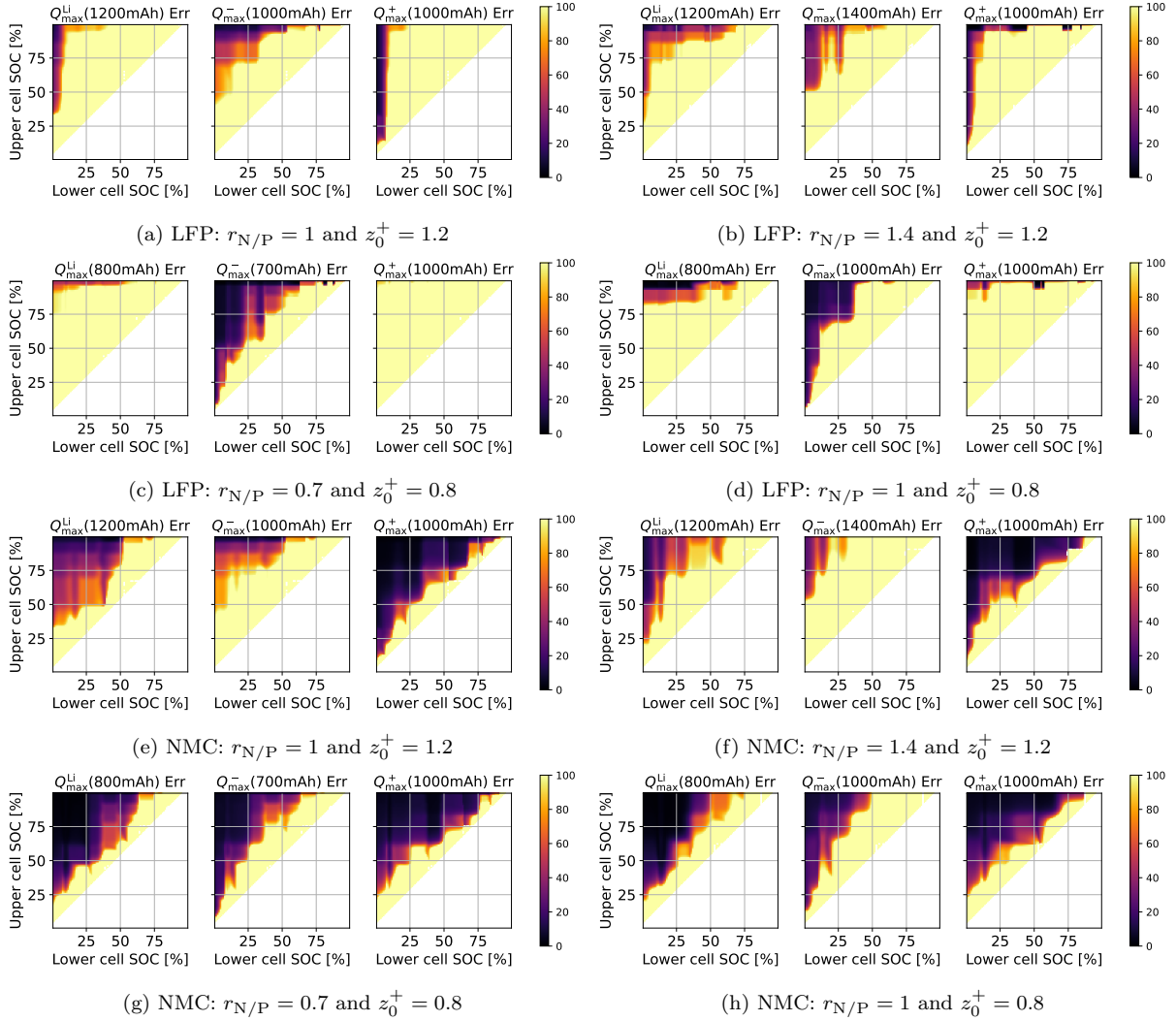


Figure 9: Standard estimation errors (in mAh shown by the color bar) of the lithium inventory  $\hat{Q}_{\text{max}}^{\text{Li}}$ , NE active materials  $\hat{Q}_{\text{max}}^-$ , and PE active materials  $\hat{Q}_{\text{max}}^+$  based on OCV measurements sampled at every charge throughput increment  $\Delta Q_c$  amounting to 1% cell SOC change. Each charge throughput window of voltage measurements is normalized into a cell SOC window  $[z_{\text{lower}}, z_{\text{upper}}]$  at least 1% apart. The errors are obtained as the square root of the diagonals of the inverse Fisher information matrix evaluated at different pairs of  $(r_{N/P}, z_0^+)$  values corresponding to the four regimes discussed in section 2.7, with  $\hat{Q}_{\text{max}}^+ = 1\text{Ah}$  being fixed in all cases. The standard OCV measurement error is assumed to be  $\sigma_U = 5\text{mV}$ . (a, b, c, d) LFP/MCMB results. (e, f, g, h) NMC/MCMB counterparts.

Besides, we can also observe that the identifiability of the active material amount in an electrode strongly depends on the intrinsic OCP relation so this particular material. For example, the active material of LFP tends to be hard to identify, likely due to the flatness and lack of features in its OCP.

In contrast, the active material of NMC is much more identifiable. Moreover, the identifiability of graphite shares a rather similar pattern whether it is matched with LFP or NMC to form a cell.

#### 4. Conclusions, Discussions, and Future Work

In this work, we study the electrode-specific OCV model assembled from the PE and NE OCP and re-parametrize a popular formulation in literature by the dimensionless N/P ratio  $r_{N/P} = \hat{Q}_{\max}^- / \hat{Q}_{\max}^+$  and the Li/P ratio  $z_0^+ = \hat{Q}_{\max}^{\text{Li}} / \hat{Q}_{\max}^+$ , which are independent, cutoff-voltage-agnostic, pristine-condition-agnostic, and intuitively linked to the lithium inventory  $\hat{Q}_{\max}^{\text{Li}}$  and active material amounts  $\hat{Q}_{\max}^\pm$ . Estimating them thus gives us important information about the degradation mode of LLI, LAMn, and LAMp. Along the way, we also clarify several confusions regarding electrode stoichiometry  $x^\pm$  versus electrode SOC  $z^\pm$ , precise meaning of cell SOC  $z$  and SOH, and their relations to the artificially specified upper and lower cutoff voltage.

We then analytically derive the sensitivity gradients of the electrode SOC limits and  $z$ -based cell OCV  $U_{\text{OCV}}(z)$  with respect to the N/P and Li/P ratio. Such analytic results not only offer a closed-form expression to easily calculate these derivatives, but the form of the expressions also provides insights into how each factor affects the parametric sensitivity. In particular, the concept of PE and NE DV fraction naturally emerges in the derivation, which characterize which electrode is dominating the OCV changes at each cell SOC and are instrumental in propagating the effects of a fixed upper and lower cutoff voltage into the sensitivity gradients. The local sensitivity delineated by these parametric derivatives are visualized and verified by simulations and comparison against empirical sensitivity results.

Furthermore, we derive the sensitivity gradients of cell total capacity  $\hat{Q}_{\max}$  with respect to the lithium inventory  $\hat{Q}_{\max}^{\text{Li}}$  and active material amounts  $\hat{Q}_{\max}^\pm$ . These dimensionless derivatives intuitively indicate to what extent each degradation mode of LLI, LAMn, and LAMp is limiting the apparent total capacity. Visualizing the pattern of their dependence on the N/P and Li/P ratio reveals four characteristic regimes regarding their identifiability.

We also demonstrate a direct application of these analytic results in practice, which regards estimating the N/P and Li/P ratio from complete OCV curve measurements using NLS and estimating lithium inventory and active material amounts from partial OCV measurements. We show how to obtain an NLS estimator error covariance from the Fisher information matrix, which directly depends on the sensitivity gradients, and how such information helps us choose an SOC window that yields informative OCV measurements.

We want to emphasize that any statements based on sensitivity gradients are only valid locally, i.e. valid for a small range of parameters around the point at which the gradients are evaluated. More empirical tools from statistical inference will be needed to discern global sensitivity, and we will report our findings in future work.

Another limitation is that we have only discussed inferring degradation modes from OCV measurements, which has a relatively restricted scope of application in practice. To go beyond OCV measurements, we need to somehow estimate the cell SOC or OCV from terminal voltage recorded in finite-current operation. This can either be done by simple  $IR_0$  corrections based on equivalent internal resistance  $R_0$  [18], or by more sophisticated model-based filtering such as in a battery management system [5].

#### Acknowledgements

J.L. and E.K. acknowledge funding by Agency for Science, Technology and Research (A\*STAR) under the Career Development Fund (C210112037).

## References

- [1] J. S. Edge, S. O’Kane, R. Prosser, N. D. Kirkaldy, A. N. Patel, A. Hales, A. Ghosh, W. Ai, J. Chen, J. Jiang, Lithium Ion Battery Degradation: What you need to know, *Physical Chemistry Chemical Physics* (2021). Publisher: Royal Society of Chemistry.
- [2] P. M. Attia, A. Bills, F. B. Planella, P. Dechent, G. d. Reis, M. Dubarry, P. Gasper, R. Gilchrist, S. Greenbank, D. Howey, O. Liu, E. Khoo, Y. Preger, A. Soni, S. Sripad, A. G. Stefanopoulou, V. Sulzer, Review—“Knees” in Lithium-Ion Battery Aging Trajectories, *Journal of The Electrochemical Society* 169 (2022) 060517. URL: <https://doi.org/10.1149/1945-7111/ac6d13>. doi:10.1149/1945-7111/ac6d13, publisher: The Electrochemical Society.
- [3] C. R. Birkl, M. R. Roberts, E. McTurk, P. G. Bruce, D. A. Howey, Degradation diagnostics for lithium ion cells, *Journal of Power Sources* 341 (2017) 373–386. URL: <https://www.sciencedirect.com/science/article/pii/S0378775316316998>. doi:10.1016/j.jpowsour.2016.12.011.
- [4] G. L. Plett, Battery management systems: Battery modeling, volume 1 of *Power engineering series*, Artech House, 2015.
- [5] G. L. Plett, Battery management systems: Equivalent-circuit methods, volume 2 of *Artech House Power engineering series*, Artech House, 2016.
- [6] D. Andre, C. Appel, T. Soczka-Guth, D. U. Sauer, Advanced mathematical methods of SOC and SOH estimation for lithium-ion batteries, *Journal of Power Sources* 224 (2013) 20–27. URL: <https://www.sciencedirect.com/science/article/pii/S0378775312015303>. doi:10.1016/j.jpowsour.2012.10.001.
- [7] M.-F. Ng, J. Zhao, Q. Yan, G. J. Conduit, Z. W. Seh, Predicting the state of charge and health of batteries using data-driven machine learning, *Nature Machine Intelligence* 2 (2020) 161–170. URL: <http://www.nature.com/articles/s42256-020-0156-7>. doi:10.1038/s42256-020-0156-7.
- [8] M. Dubarry, C. Truchot, B. Y. Liaw, Synthesize battery degradation modes via a diagnostic and prognostic model, *Journal of Power Sources* 219 (2012) 204–216. URL: <https://www.sciencedirect.com/science/article/pii/S0378775312011330>. doi:10.1016/j.jpowsour.2012.07.016.
- [9] J. Z. Olson, C. M. López, E. J. F. Dickinson, Differential Analysis of Galvanostatic Cycle Data from Li-Ion Batteries: Interpretative Insights and Graphical Heuristics, *Chemistry of Materials* 35 (2023) 1487–1513. URL: <https://doi.org/10.1021/acs.chemmater.2c01976>. doi:10.1021/acs.chemmater.2c01976, publisher: American Chemical Society.
- [10] H. M. Dahn, A. J. Smith, J. C. Burns, D. A. Stevens, J. R. Dahn, User-Friendly Differential Voltage Analysis Freeware for the Analysis of Degradation Mechanisms in Li-Ion Batteries, *Journal of The Electrochemical Society* 159 (2012) A1405. URL: <https://iopscience.iop.org/article/10.1149/2.013209jes/meta>. doi:10.1149/2.013209jes, publisher: IOP Publishing.



- [11] P. Mohtat, S. Lee, J. B. Siegel, A. G. Stefanopoulou, Towards better estimability of electrode-specific state of health: Decoding the cell expansion, *Journal of Power Sources* 427 (2019) 101–111. URL: <https://www.sciencedirect.com/science/article/pii/S0378775319303593>. doi:10.1016/j.jpowsour.2019.03.104.
- [12] V. Sulzer, S. G. Marquis, R. Timms, M. Robinson, S. J. Chapman, Python Battery Mathematical Modelling (PyBaMM), *Journal of Open Research Software* 9 (2021) 14. URL: <http://openresearchsoftware.metajnl.com/articles/10.5334/jors.309/>. doi:10.5334/jors.309.
- [13] C. Pastor-Fernández, T. F. Yu, W. D. Widanage, J. Marco, Critical review of non-invasive diagnosis techniques for quantification of degradation modes in lithium-ion batteries, *Renewable and Sustainable Energy Reviews* 109 (2019) 138–159. URL: <https://www.sciencedirect.com/science/article/pii/S136403211930200X>. doi:10.1016/j.rser.2019.03.060.
- [14] R. Xu, Y. Wang, Z. Chen, Data-Driven Battery Aging Mechanism Analysis and Degradation Pathway Prediction, *Batteries* 9 (2023) 129. URL: <https://www.mdpi.com/2313-0105/9/2/129>. doi:10.3390/batteries9020129.
- [15] S. Lee, P. Mohtat, J. B. Siegel, A. G. Stefanopoulou, J.-W. Lee, T.-K. Lee, Estimation Error Bound of Battery Electrode Parameters With Limited Data Window, *IEEE Transactions on Industrial Informatics* 16 (2020) 3376–3386. doi:10.1109/TII.2019.2952066.
- [16] I. Bloom, A. N. Jansen, D. P. Abraham, J. Knuth, S. A. Jones, V. S. Battaglia, G. L. Henriksen, Differential voltage analyses of high-power, lithium-ion cells: 1. Technique and application, *Journal of Power Sources* 139 (2005) 295–303. URL: <https://www.sciencedirect.com/science/article/pii/S0378775304008146>. doi:10.1016/j.jpowsour.2004.07.021.
- [17] M. Dubarry, D. Beck, Perspective on Mechanistic Modeling of Li-Ion Batteries, *Accounts of Materials Research* 3 (2022) 843–853. URL: <https://pubs.acs.org/doi/10.1021/accountsmr.2c00082>. doi:10.1021/accountsmr.2c00082.
- [18] J. Schmitt, M. Rehm, A. Karger, A. Jossen, Capacity and degradation mode estimation for lithium-ion batteries based on partial charging curves at different current rates, *Journal of Energy Storage* 59 (2023) 106517. URL: <https://www.sciencedirect.com/science/article/pii/S2352152X22025063>. doi:10.1016/j.est.2022.106517.
- [19] M. Dubarry, M. Bercibar, A. Devie, D. Anseán, N. Omar, I. Villarreal, State of health battery estimator enabling degradation diagnosis: Model and algorithm description, *Journal of Power Sources* 360 (2017) 59–69. URL: <https://linkinghub.elsevier.com/retrieve/pii/S0378775317307723>. doi:10.1016/j.jpowsour.2017.05.121.
- [20] M. Dubarry, D. Anseán, Best practices for incremental capacity analysis, *Frontiers in Energy Research* 10 (2022) 1023555. URL: <https://www.frontiersin.org/articles/10.3389/fenrg.2022.1023555/full>. doi:10.3389/fenrg.2022.1023555.
- [21] M. Dubarry, V. Agrawal, M. Hüske, M. Kuipers, Accurate LLI and LAM<sub>pe</sub> Estimation Using the Mechanistic Modeling Approach with Layered Oxides, *Journal of The Electrochemical Society* 170 (2023) 070503. URL: <https://iopscience.iop.org/article/10.1149/1945-7111/ace21c>. doi:10.1149/1945-7111/ace21c.

- [22] A. J. Smith, J. C. Burns, D. Xiong, J. R. Dahn, Interpreting High Precision Coulometry Results on Li-ion Cells, *Journal of The Electrochemical Society* 158 (2011) A1136. URL: <https://iopscience.iop.org/article/10.1149/1.3625232/meta>. doi:10.1149/1.3625232, publisher: IOP Publishing.
- [23] M.-T. F. Rodrigues, Capacity and Coulombic Efficiency Measurements Underestimate the Rate of SEI Growth in Silicon Anodes, *Journal of The Electrochemical Society* 169 (2022) 080524. URL: <https://dx.doi.org/10.1149/1945-7111/ac8a21>. doi:10.1149/1945-7111/ac8a21, publisher: IOP Publishing.
- [24] J. Schmitt, M. Schindler, A. Oberbauer, A. Jossen, Determination of degradation modes of lithium-ion batteries considering aging-induced changes in the half-cell open-circuit potential curve of silicon-graphite, *Journal of Power Sources* 532 (2022) 231296. URL: <https://www.sciencedirect.com/science/article/pii/S0378775322003123>. doi:10.1016/j.jpowsour.2022.231296.
- [25] A. Tornheim, D. C. O'Hanlon, What do Coulombic Efficiency and Capacity Retention Truly Measure? A Deep Dive into Cyclable Lithium Inventory, Limitation Type, and Redox Side Reactions, *Journal of The Electrochemical Society* 167 (2020) 110520. URL: <https://dx.doi.org/10.1149/1945-7111/ab9ee8>. doi:10.1149/1945-7111/ab9ee8, publisher: IOP Publishing.
- [26] M. D. Berliner, H. Zhao, S. Das, M. Forsuelo, B. Jiang, W. Chueh, M. Z. Bazant, R. D. Braatz, Nonlinear Identifiability Analysis of the Porous Electrode Theory Model of Lithium-Ion Batteries, *Journal of The Electrochemical Society* (2021). URL: <https://iopscience.iop.org/article/10.1149/1945-7111/ac26b1>. doi:10.1149/1945-7111/ac26b1.
- [27] A. Ly, M. Marsman, J. Verhagen, R. Grasman, E.-J. Wagenmakers, A Tutorial on Fisher Information, 2017. URL: <http://arxiv.org/abs/1705.01064>, arXiv:1705.01064 [math, stat].
- [28] T. M. Cover, J. A. Thomas, *Elements of information theory*, 2nd ed ed., Wiley-Interscience, Hoboken, N.J, 2006.